nature microbiology

Article

https://doi.org/10.1038/s41564-026-02444-x

Combination therapy with broadly neutralizing antibodies, antiretroviral therapy and CCR5 blockade limits viral reservoir seeding in infant macaque model of HIV

Received: 18 November 2025

Accepted: 7 July 2026

Published online: 10 August 2026

Check for updates

Jonah B. Sacha[1,2] ✉, Tracy Ordonez[1], Shilpi Pandey[1], Gabriela Webb[1], Philip Barnette[1], Cleiton Pessoa[1], Matthew C. Humkey[1], Jason Reed[1], Anden Morehead[1], Jennifer K. Watanabe[3], Jodie L. Usachenko[3], Shrivaas Vijayan[3], Altair Fazio[1], Heather Sidener[1], Anne D. Lewis[1], Gabrielle Pastenkos[3], Sohita Ojha[1], Aaron Barber-Axthelm[1], Bella Swan[1], Rachele Bochart[1], John R. Mascola[4,8], Amarendra Pegu[4], Emily J. Fray[5], Rachael M. Wolters[1], Janet D. Siliciano[5], Robert F. Siliciano[6], Scott G. Hansen[1,2], Koen K. A. Van Rompay[3,7], Ann J. Hessell[1] & Nancy L. Haigwood[1] ✉

Lack of access to antiretroviral therapy (ART) leads to the transmission of human immunodeficiency virus in ~120,000 children annually, emphasizing the need for new strategies to prevent lifelong infection. Here in an infant rhesus macaque model of peripartum oral infection, we show that broadly neutralizing antibodies directed to the viral envelope protein were insufficient to prevent latent reservoir establishment, independent of daily ART. Blockade of the human immunodeficiency virus co-receptor CCR5 via the antibody leronlimab also failed to prevent reservoir establishment, but it significantly reduced reservoir seeding in lymphoid and gastrointestinal tissues. Following the treatment of infants with viraemia at 72 h post-infection with the combination of broadly neutralizing antibodies, ART and leronlimab, no subsequent evidence of replicating or latent virus and antiviral immunity was observed 1 year after treatment interruption. These findings suggest a synergy between broadly neutralizing antibodies, ART and CCR5 blockade for preventing viral reservoir establishment and offer potential improvements over current therapies for newborns exposed to human immunodeficiency virus.

Treatment of human immunodeficiency virus (HIV) infection with combinations of antiretroviral therapy (ART) drugs has led to longer lives in both adults and children living with HIV (CLWH), but even decades of ART have failed to clear the reservoir[1]. HIV-induced disease is exacerbated in CLWH compared with adults, leading to 50% mortality by 1 year of life if untreated[2]. Even with ART, CLWH suffer increased comorbidities owing to ongoing immune dysfunction and inflammation[3]. Thus, interventions targeted to prevent the establishment or clearance of the latent viral reservoir in CLWH are needed.

HIV broadly neutralizing antibodies (bNAbs) targeting the HIV envelope (Env) protein are promising therapeutics for the treatment of HIV[4–6]. Although bNAbs can control viraemia in people living with HIV, these treatments cannot clear HIV infection once the viral reservoir is set[7,8]. Orthogonal to bNAbs, leronlimab (LRM) is a humanized monoclonal IgG4 antibody targeting the N-terminus and extracellular

A full list of affiliations appears at the end of the paper. ✉e-mail: sacha@ohsu.edu; haigwoon@ohsu.edu

loop-2 of the HIV co-receptor CCR5. LRM has shown antiviral activity in people living with HIV, is well tolerated in treated individuals[9,10] and was shown to prevent acquisition of chimeric simian–HIV (SHIV) bearing a CCR5-tropic HIV Env in macaques[11].

Nonhuman primate models for AIDS using simian immunodeficiency virus (SIV) accurately model the dynamics of reservoir establishment[12,13] and rebound following analytical treatment interruption (ATI)[14]. In juveniles, treatment with ART beginning at 72 h onwards consistently led to viral rebound, whereas earlier treatment limited viral seeding[15]. Oral infection with SIV or SHIV in infant rhesus macaques between 0 and 16 weeks of age resulted in high, persistent viraemia and rapid pathogenesis and disease progression requiring euthanasia in 50% of infant macaques within 4 to 6 months of infection[16], similar to that observed in untreated newborns who acquired HIV during childbirth[17,18]. Similarly, treatment with a mixture of two bNAbs initiated 30–48 h after oral SHIV exposure prevented the establishment of a permanent viral reservoir[19]. One-time dosing with a bolus of bNAbs resulted in better viral clearance and substantially reduced anti-drug antibody (ADA) responses compared with four doses distributed over 10 days. This limited window of opportunity in infants (≤48 h) underscores the importance of very early intervention to limit the size of the reservoir and that bNAbs can be a powerful antiviral tool[6].

In the current work, we performed a systematic evaluation of individual, dual and three-way combined treatments of relatively short duration in SHIV-infected infant macaques using agents with different mechanisms of action. These treatments were initiated at 72 h after oral virus inoculation, when primary viraemia was measurable in the plasma, and when none of the individual treatments alone could prevent subsequent viral rebound after ART cessation. Our goal was to test the hypothesis that blockage of CCR5 by LRM in combination with bNAbs targeting the viral Env protein and ART would effectively prevent viral spread to new target cells and may prevent reservoir establishment. These results suggest a strategy for early treatment that may be effective in leading to a functional or complete cure.

Results

Early treatment with bNAbs to define the window of opportunity

We designed a series of individual, dual and triple combination post-exposure antiviral therapy experiments in rhesus macaque infants orally exposed to high-dose $SHIV_{SF162P3}$, an SIVmac239 virus encoding an HIV Env that was passaged in vivo and is exceptionally pathogenic in infant macaques. Infection results in 50% of animals progressing to AIDS-like disease and clinical endpoints by 12 weeks post-infection without treatment[16], very similar to studies with SIVmac251 in orally infected infant macaques[20]. The study included 55 male and female infant macaques in groups of 6 to 8 in a systematic comparison of treatments (Fig. 1a and Supplementary Table 1). Seven historical and contemporaneous untreated controls were sampled weekly for up to 25 weeks after SHIV oral infection, and viral RNA copies per millilitre of plasma were quantified by RT-PCR (Fig. 1b). As the primary readout for infection, we measured plasma viral RNA loads (PVLs) and cell-associated viral DNA loads (CAVLs) in peripheral blood mononuclear cells (PBMCs) (Extended Data Fig. 1), and we compared these values with plasma bNAb concentrations (Supplementary Fig. 1) as a function of time after exposure to virus. In addition, lymph nodes (LNs) were biopsied at various times after infection to quantify viral RNA and DNA, and multiple tissues were tested for total viral copies at the time of euthanasia.

Treatment with bNAbs VRC07-523LS and PGT121 at 24 and 30 h after oral virus exposure was shown previously to fully clear SHIV infection in both the blood and 15 gut and lymphoid tissues taken at necropsy[19,21]. To expand the window of opportunity for bNAbs alone, we injected a bolus of the bNAb cocktail consisting of 20 mg kg^{-1} each of PGT121 and VRC07-523LS initiated 48 h after SHIV infection. This treatment resulted in therapeutic antibody levels in plasma and eliminated the virus in 5/6 animals, and in the remaining animal, it increased the time to rebound, decreased set-point viraemia and resulted in the development of adaptive immunity (Fig. 1c and Supplementary Fig. 1). $CD8^+$ T-cell depletion was performed at week 22 of the study, and only this single animal (RM10) showed rebound of PVL, which returned to $<10^4$ copies per ml when $CD8^+$ cells were restored in the periphery. By contrast, delivery of the antibody mixture at 72 h post-infection was successful in blunting primary viraemia, but resulted in viral rebound in 4 infants at weeks 5 and 6, with the other 2 rebounding at weeks 16 and 22, concomitant with waning antibody levels (Fig. 1d and Supplementary Fig. 1). We explored whether the addition of a short course of ART (21 days) could improve the effectiveness of bNAbs started at 72 h, and we compared a 21-day course of ART (Fig. 1e) with the combination of ART and bNAbs (Fig. 1f). These treatments were only modestly more effective at delaying or preventing rebound (Fig. 1g), with 2/6 animals in each group below the limit of detection with episodic viral blips. At the time of euthanasia, lymphoid and gut tissues were collected and analysed for CAVLs (Supplementary Table 2). These data corroborated cell-associated viral copy findings in the PBMCs, with 2/6 infants below or just at the limit of detection in PBMCs and tissues (Extended Data Fig. 1). Taken together, these experiments show that bNAbs given as a bolus at 48 h greatly suppresses or clears viraemia in all 6 animals but that treatment at 72 h with a bolus of bNAbs, 3 weeks of daily ART or the 2 combined is insufficient to prevent seeding in all tissues or to clear the virus in all animals.

Treatment with LRM at 72 h reduces viral seeding but does not clear infection

To test the hypothesis that inhibiting access to CCR5 on target cells could limit the seeding of new viral foci, we treated infants with repeated weekly doses of LRM beginning at 72 h post-infection (Fig. 2a). To rapidly achieve and maintain full CCR5 receptor occupancy (RO), we initiated treatment with weekly 50 mg kg^{-1} LRM and then switched to a weekly 10 mg kg^{-1} dose, which represent allometrically scaled macaque versions of the human 700 mg and 350 mg doses, respectively[11]. As expected, this dosing regimen resulted in high plasma levels of LRM and full CCR5 RO on the surface of $CD4^+$ T cells in peripheral blood through the first 32 weeks of infection (Supplementary Fig. 2). Weekly LRM treatment for 28 weeks resulted in 2–4 $\log_{10}$ reduction in steady-state levels of virus in plasma, with 3/6 infants reaching undetectable PVL by the end of the treatment window (Fig. 2b). Plasma virus then increased modestly after the decay of the antibody in the plasma and loss of CCR5 RO. LRM monotherapy did not prevent reservoir establishment, as all six LRM-treated infants had reduced but detectable cell-associated virus in PBMCs (Fig. 2c). Suppression of viraemia suggests that reducing seeding is beneficial but that LRM alone, even over an extended period, is insufficient when initiated at 72 h. We next tested a shorter course of LRM consisting of 6 weekly infusions of 50 mg kg^{-1}, followed by 2 weekly infusions of 10 mg kg^{-1}, combined with a 27-week course of ART to limit viral replication until LRM clearance. Similar to the outcome of treatment with ART + bNAbs, acute-phase viraemia was blunted with no evidence of cell-associated virus present in PBMCs (Fig. 2d,e). However, once ART was discontinued following LRM washout and loss of CCR5 RO (Supplementary Fig. 2), virus rebounded in 4/6 animals, with a delay of 9–10 weeks in both the plasma virus and cell-associated PBMC virus in 3 of the rebounding animals. Therefore, both bNAbs and LRM in combination with ART at 72 h post-infection were insufficient to prevent the establishment of infection.

Given the critical role of CCR5 as the major HIV co-receptor in mucosal transmission, we next assessed whether LRM-mediated inhibition of CCR5 early after infection impacted the initial seeding of the viral reservoir in lymphoid or gastrointestinal tissues. Lymphoid and gut tissues obtained at necropsy were analysed for CAVLs (Supplementary Table 2). The two animals in the combined LRM plus ART group that did not rebound (RM41 and RM43) had tissue levels that were at or below the limit of detection. Within lymphoid tissues,

https://doi.org/10.1038/s41564-026-02444-x

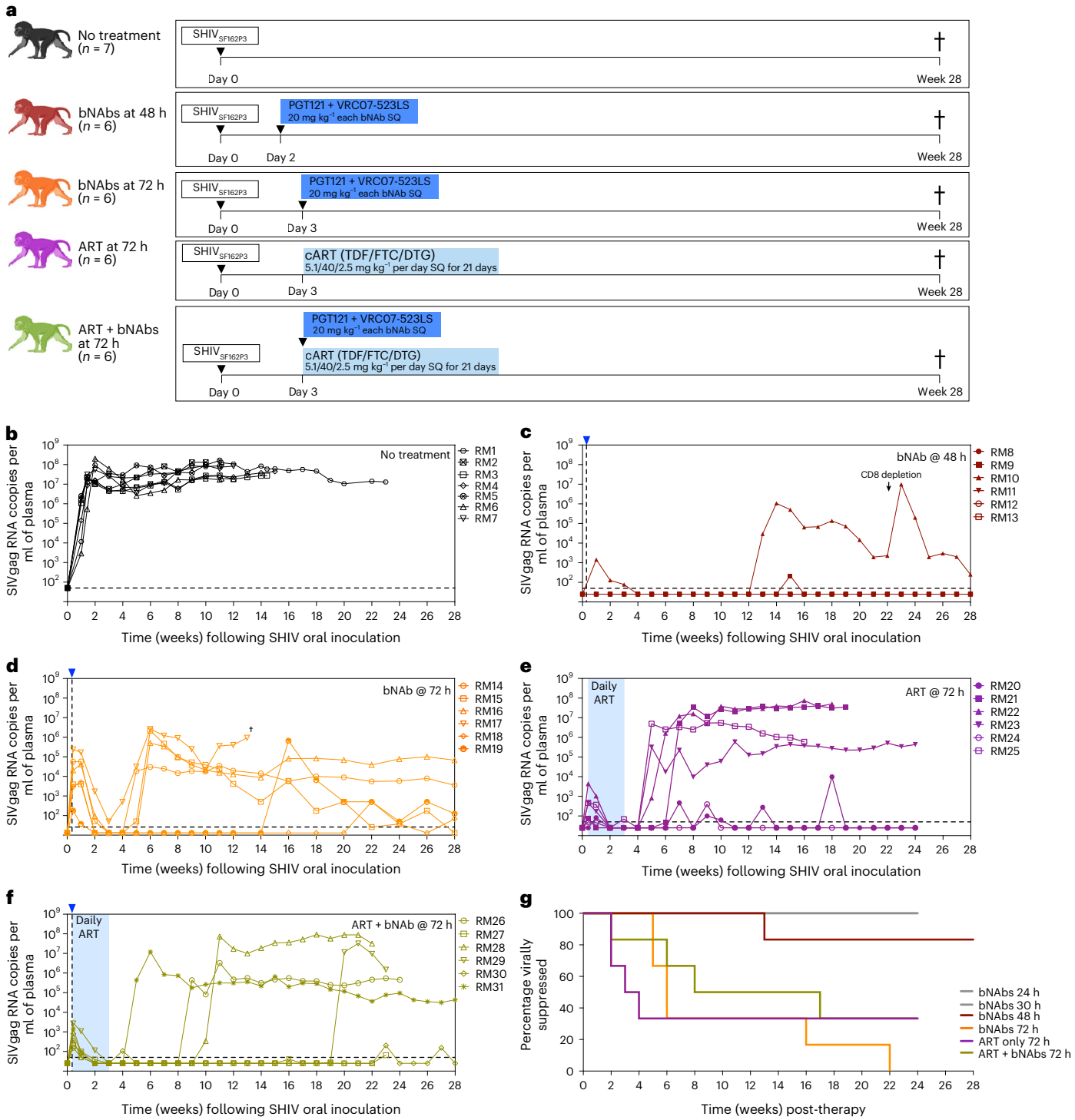

Fig. 1 | Defining the window of opportunity for early bNAb and ART treatment in infants. a, Study design. Infant rhesus macaques (1 month old) were exposed to a single high-dose $SHIV_{SF162P3}$ challenge by atraumatic oral inoculations. SQ, subcutaneous delivery. TDF (5.1 mg kg^{-1}), FTC (40 mg kg^{-1}) and DTG (2.5 mg kg^{-1}). Cross at 28 weeks indicates time of necropsy. **b**, No treatment controls ($n = 7$). **c**, PGT121 and VRC07-523LS administered subcutaneously at 20 mg kg^{-1} each at 48 h post-infection ($n = 6$). Time of $CD8^+$ cell depletion is noted with arrow at week 22. **d**, PGT121 and VRC07-523LS administered subcutaneously at 20 mg kg^{-1} each at 72 h post-infection ($n = 6$). **e**, cART initiated at 72 h post-infection for 21 days ($n = 6$). **f**, PGT121 and VRC07-523LS administered subcutaneously at 20 mg kg^{-1} each at 72 h post-infection in addition to cART initiation at 72 h post-infection for 21 days ($n = 6$). In **b**–**f**, plasma viral loads were measured longitudinally. Horizontal dashed line indicates limit of detection of 50 SIV gag RNA copies per ml. Vertical dashed line and blue arrow indicate bNAb administration. Blue box indicates time on cART. **g**, Kaplan–Meier curve showing the percentage of animals that remained virally suppressed post-therapy based on plasma viral loads. Data for treatment at 24 h[21] and 30 h[19] (grey line) were published previously. Schematic in **a** created in BioRender; Webb, G. https://biorender.com/xowloj9 (2026).

LRM treatment resulted in a 1 log_{10} reduction in CAVLs compared with ART alone or ART plus bNAbs (Fig. 2f). Within gastrointestinal tissues, LRM, alone or in combination with ART, resulted in a 1 log_{10} reduction in CAVLs compared with ART alone or ART plus bNAbs (Fig. 2g). These data demonstrated that LRM-mediated CCR5 blockade in acute infection limits reservoir seeding in both lymphoid and gastrointestinal tissues and suggested that this effect may be amplified when combined with other antiviral treatments such as bNAbs.

https://doi.org/10.1038/s41564-026-02444-x

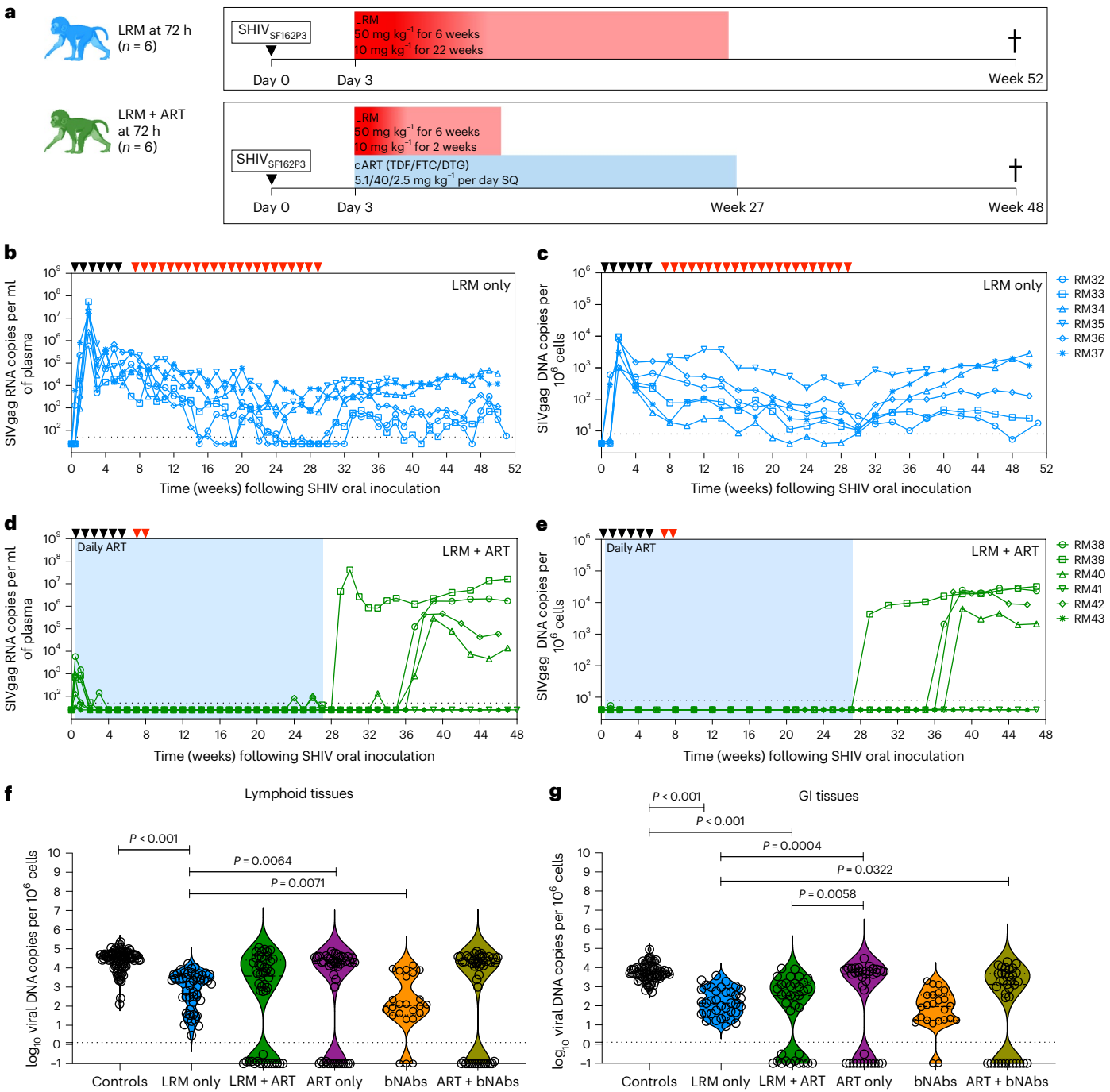

Fig. 2 | Characterization of viraemia following LRM treatment. a, Study design. Infant rhesus macaques (1 month old) were exposed to a single high-dose $SHIV_{SF162P3}$ challenge by atraumatic oral inoculations. TDF (5.1 mg kg^{-1}), FTC (40 mg kg^{-1}) and DTG (2.5 mg kg^{-1}). Cross indicates time of necropsy. **b**,**c**, LRM administered subcutaneously at 72 h post-infection at 50 mg kg^{-1} for 6 weeks and then 10 mg kg^{-1} for 22 weeks ($n = 6$). **d**,**e**, LRM administered subcutaneously at 72 h post-infection at 50 mg kg^{-1} for 6 weeks and then 10 mg kg^{-1} for 2 weeks in addition to cART initiation at 72 h post-infection for 27 weeks ($n = 6$). In **b** and **d**, plasma viral loads were measured longitudinally. Horizontal dashed line indicates limit of detection of 50 SIV gag RNA copies per ml. In **c** and **e**, CAVLs from PBMCs were also measured longitudinally. Horizontal dashed line indicates limit of detection of 8 SIV gag DNA copies per 10^6 cells. Black and red arrows indicate LRM administration at 50 and 10 mg kg^{-1}, respectively. Blue box indicates time on cART. **f**, Viral DNA copies at time of necropsy in various lymphoid tissues (retropharyngeal, submandibular, tracheobronchial, axillary, mixed mesenteric, iliosacral and inguinal LNs, and tonsil). **g**, Viral DNA copies at time of necropsy in various gastrointestinal tissues (descending colon, duodenum, ileum, jejunum, rectum and cecum). *P* values were calculated using two-way ANOVA and mixed-effect analysis with Tukey's multiple comparison test. $^*P < 0.05$, $^{**}P < 0.01$, $^{***}P < 0.001$ and $^{****}P < 0.0001$. GI, gastrointestinal. Schematic in **a** created in BioRender; Webb, G. https://biorender.com/pdl5850 (2026).

Triple therapy prevents viral reservoir seeding and post-treatment rebound

We next tested the efficacy of a triple therapy consisting of LRM (6 weekly infusions of 50 mg kg^{-1}, followed by 3 weekly infusions of 10 mg kg^{-1}), bNAbs (20 mg kg^{-1} each of VRC07-523LS and PGT121) and 27 weeks of ART beginning at 72 h post-infection in 8 orally SHIV-infected infants (Fig. 3a). This LRM dosing strategy was selected to rapidly achieve full CCR5 RO that then decayed with kinetics similar to bNAb

https://doi.org/10.1038/s41564-026-02444-x

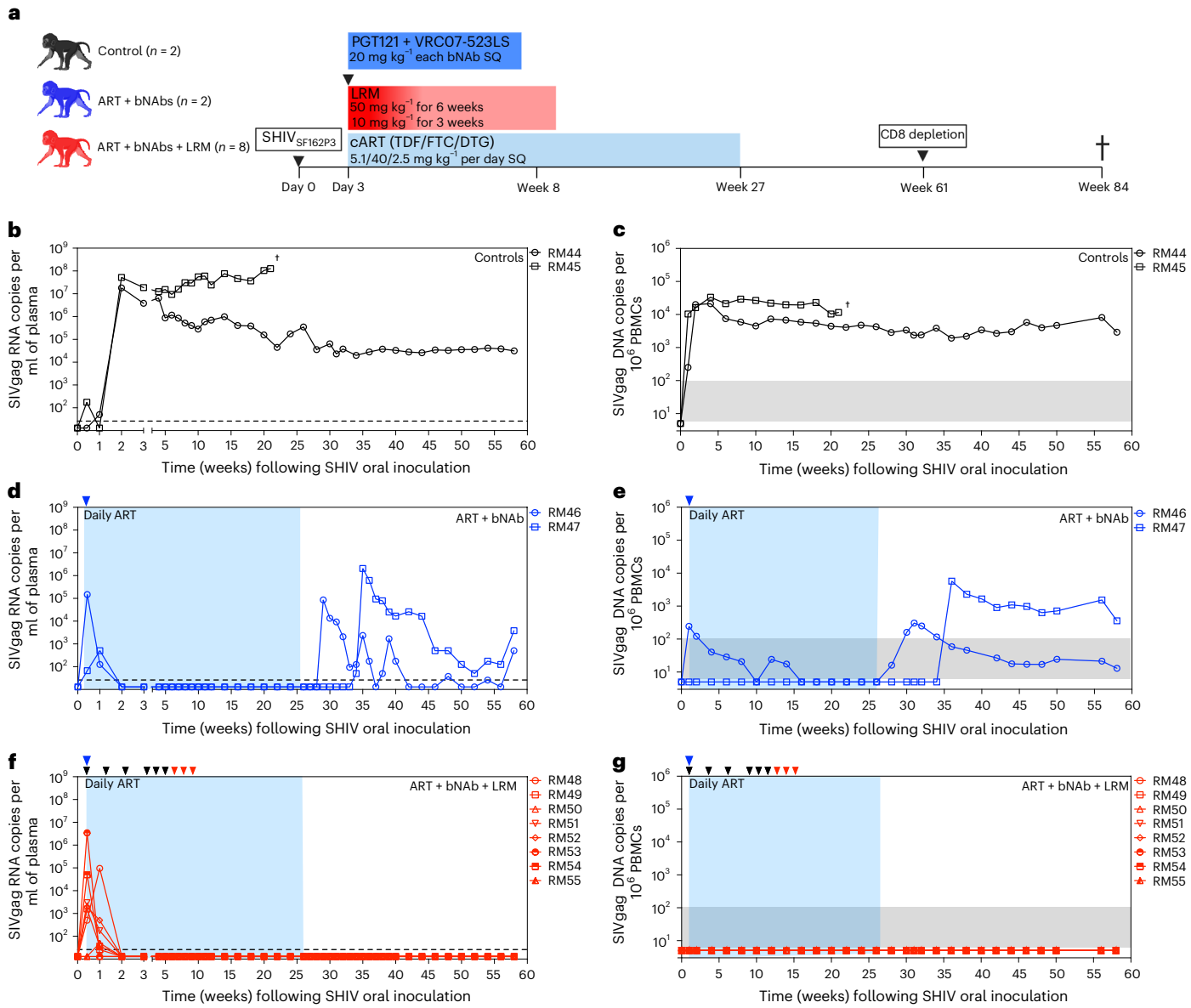

Fig. 3 | Triple therapy prevents viral reservoir seeding and post-treatment rebound. a, Study design. Infant rhesus macaques (1 month old) were exposed to a single high-dose $SHIV_{SF162P3}$ challenge by atraumatic oral inoculations. TDF (5.1 mg kg^{-1}), FTC (40 mg kg^{-1}) and DTG (2.5 mg kg^{-1}). Cross indicates time of necropsy. **b**,**c**, No treatment controls ($n = 2$). **d**,**e**, PGT121 and VRC07-523LS administered subcutaneously at 20 mg kg^{-1} each at 72 h post-infection in addition to cART initiation at 72 h post-infection for 27 weeks ($n = 2$). **f**,**g**, PGT121 and VRC07-523LS administered subcutaneously at 20 mg kg^{-1} each at 72 h post-infection; LRM administered subcutaneously at 72 h post-infection at 50 mg kg^{-1} for 6 weeks and then 10 mg kg^{-1} for 3 weeks in addition to cART initiation at 72 h post-infection for 27 weeks ($n = 8$). In **b**, **d** and **f**, plasma viral loads were measured longitudinally. Horizontal dashed line indicates limit of detection of 26 SIV gag RNA copies per ml. In **c**, **e** and **g**, CAVLs from PBMCs were also measured longitudinally. Grey box indicates a limit of detection range of 5–100 SIV gag DNA copies per 10^6 cells. Black and red arrows indicate LRM administration at 50 and 10 mg kg^{-1}, respectively. Blue arrows indicate bNAb administration. Blue box indicates time on cART. Schematic in **a** created in BioRender; Webb, G. https://biorender.com/mq7uoxi (2026).

clearance in blood. We included two untreated SHIV-inoculated controls and two SHIV-inoculated infants treated with daily ART for 27 weeks plus the same bNAb bolus described above, initiated at 72 h to confirm that previous experimental outcomes were still observed with the longer 27-week ART treatment course needed to account for LRM washout. As expected, both untreated controls progressed with uncontrolled viraemia and high levels of cell-associated viral DNA in PBMC, with one of the control infants requiring euthanasia at 20 weeks owing to AIDS-related illness (Fig. 3b,c). In the two ART plus bNAb-treated infants, viraemia was rapidly suppressed and remained undetectable until ART interruption at week 27 (Fig. 3d). Following ATI, virus in one infant rebounded immediately with a peak of 10^5 copies per ml, whereas virus in the second infant rebounded 7 weeks later with a peak of 10^6 copies per ml. In line with this post-ATI rebound, cell-associated viral DNA was detected in the PBMCs in the infant that had 10^5 copies per ml at time of therapy initiation (Fig. 3e). All eight triple therapy-treated infants had detectable viraemia at time of treatment initiation that was rapidly suppressed through week 27 (Fig. 3f and Extended Data Fig. 2). In contrast to the untreated controls, there was no consistent loss of $CD4^+$ T cell in peripheral blood of the two ART plus bNAb-treated infants or the eight triple therapy-treated infants (Extended Data Fig. 3). Once washout of bNAbs, LRM and CCR5 RO was confirmed (Extended Data Fig. 4), ART treatment was interrupted at week 27. Surprisingly, all eight infants remained aviraemic through 6 months of follow-up after ATI (Fig. 3f). Despite high levels of acute-phase viraemia, no cell-associated viral DNA was detected in

the PBMCs or tissues of any animal throughout the entire monitoring period by either quantitative PCR or in situ hybridization (Fig. 3g, Extended Data Fig. 5 and Supplementary Table 2). These data raised the possibility that the triple therapy completely prevented the establishment of the permanent viral reservoir.

To assess for the presence of latent virus, at week 56 post-infection, we assayed for antiviral CD8$^+$ T immunity in PBMCs and LNs, and for the presence of CAVLs in isolated CD4$^+$ T cells from LNs before CD8$^+$ cell depletion at week 61. Despite readily measuring Gag-specific CD8$^+$ T cells in the single living control animal and the two bNAb + ART animals, there were no Gag-specific CD8$^+$ T cells observed in any of the eight triple therapy-treated infants (Fig. 4a). Mirroring the cellular immune responses, we observed antibodies binding to HIV-SF162 Env in the two bNAb + ART animals, but not in any of the eight triple therapy-treated infants (Supplementary Fig. 3). Cell-associated viral DNA was not detected in peripheral blood or LN CD4$^+$ T cells isolated from the eight triple therapy-treated infants (Fig. 4b). Following CD8$^+$ cell depletion with an anti-CD8 alpha antibody at week 61 (Supplementary Fig. 4), the single living control animal and the two bNAb + ART animals had detectable increases in viraemia and detectable CAVLs during CD8$^+$ cell depletion, which was resolved following the return of CD8$^+$ cells to pre-treatment levels (Fig. 4c–f). In stark contrast, no viral rebound in plasma or cell-associated DNA was observed in any of the eight triple therapy-treated infants during CD8 depletion (Fig. 4g,h). At week 84 post-infection, all animals were euthanized, and all tissues were examined for residual cell-associated viral DNA. Although viral DNA was found in the control and bNAb + ART infants, no sample from any of the eight triple therapy-treated infants was positive for virus nucleic acid (Fig. 4i and Extended Data Fig. 5). To further search for virus in the eight triple therapy-treated infants, CD4$^+$ T cells from lymphoid tissues were assayed for intact and defective proviruses via intact proviral DNA assay (IPDA), and no defective or intact proviruses were detected in any samples (Fig. 4j). Cumulatively, these results indicated that the triple therapy prevented seeding of the latent reservoir in infants treated at 72 h post-infection. Importantly, the triple therapy regimen was well tolerated with no clinical concerns based on daily routine health monitoring; no impact on neonatal development, as measured by weight gain, was observed compared with uninfected infants (Supplementary Fig. 5). Similarly, gross and microscopic findings for these animals were consistent with normal uninfected infant macaques in the colony, with no evidence of SHIV-related pathology. By contrast, the SHIV-infected infants in the untreated control group and the treated animals with viral rebound showed the typical pathologies associated with this pathogenic SHIV[19] (Supplementary Table 3).

Discussion

The main rationale for this research was to model relatively short-term treatments for HIV that could severely limit or clear the viral reservoir in neonates and infants in an attempt to 'cure' the infection. Here we showed that combination treatments using products currently in human clinical trials can mediate durable viral suppression or clearance of SHIV in infant rhesus macaques when initiated as late as 72 h following oral exposure/infection. This suppression does not seem to be immune-mediated, but rather mediated by the reduction of or the absence of a permanent viral reservoir. A major strength of the study is the systematic comparison of seven different treatment modalities in 55 age-matched rhesus macaque infants infected with a highly characterized, pathogenic strain of SHIV that is difficult to neutralize in vitro. One limitation of the study is the intervention at 72 h after oral virus inoculation, a time when the virus is in the process of being distributed to tissues and before the peak of viraemia. We recognize that this is a very early time in infection, but numerous studies have shown that there is very rapid dissemination of virus into distal tissues of rhesus macaques after oral exposure to SIV in juveniles[22] and infants[23] and oral exposure to SHIV in infants[24] and newborns[18]. Notably, the SHIV$_{SF162P3}$ viral inoculum was titrated in vivo to produce 100% infection[19] in newborn and infant rhesus macaque oral exposures. In the peripartum period, human newborns are exposed to HIV by swallowing or conjunctival exposure to cervicovaginal fluids, where HIV DNA levels in the mother are correlated with transmission[25]. If there are differences in kinetics or a delay in dissemination to other tissues (for example, owing to lower initial viral exposure), there could be a larger window of opportunity to intervene effectively in newborns. There is growing evidence that very early treatment of newborns using ART within days of birth can lead to reductions in the HIV viral reservoir[26], supporting results in this and other published nonhuman primate studies.

We do not know the precise mechanism of action of this triple therapy strategy, but there is a large body of clinical and safety data for each of the individual approaches, and we know[9,27,28] the limits of each of these therapies. It is clear that bNAbs alone can be highly effective as long as they persist[6], but their relatively short half-lives mean that bNAbs as therapies would need to be given repeatedly, as in the Antibody Mediated Prevention (AMP) trial[5], or be delivered by another mechanism, such as adeno-associated virus (AAV)-mediated long-term expression[29,30]. However, there is no direct evidence of bNAb-mediated killing of infected cells. We nonetheless decided to include the bNAb bolus in the triple therapy experiment and accompanying bNAb + ART controls, and reductions in tissue seeding and plasma virus were corroborated in these two additional ART + bNAb-treated animals. Finally, although LRM alone did not eradicate the virus, it significantly reduced the viral reservoir in the gastrointestinal tract, a critical source of rebound virus in SIV-infected animals[31]. These results are in line with a previous study that used a CCR5 vaccine to generate CCR5-specific antibodies in macaques, which significantly protected a subset of animals from the establishment of a long-lived reservoir[32]. Although the exact combinatorial mechanism of LRM with bNAbs remains unknown, we speculate that LRM not only inhibits viral access to the CCR5 co-receptor, thereby providing another layer of neutralization with bNAbs, but also modulates the trafficking of CD4$^+$ T-cell lymphocytes during hyperacute infection. Indeed, we have previously reported an increase of CCR5$^+$CD4$^+$ T cells in peripheral blood following LRM treatment in macaques, likely owing to interference with CCR5-mediated chemotaxis into gastrointestinal tissues[11,33]. In further support of this concept, maraviroc-mediated CCR5 inhibition reduces the incidence of visceral graft-versus-host disease following allogeneic stem cell transplantation by preventing chemotaxis of CCR5$^+$ T cells to these anatomical locations[34,35]. Therefore, future studies aimed at testing the role of CCR5-mediated lymphocyte trafficking following HIV infection are warranted. It also remains possible that LRM synergizes with bNAbs to enhance neutralization via a currently undefined mechanism. In support of this, a previous study of bi-specific antibodies reported enhancement of HIV neutralization by some, but not all, bNAbs when one arm was derived from LRM[36].

Fig. 4 | Immunological and viral reservoir analyses. a, CD8$^+$ T-cell responses at week 56 post-infection in PBMCs and LN cells specific for SIV gag; staphylococcal enterotoxin B (SEB) was used as a control. See Extended Data Fig. 6 for gating strategy. **b**, CAVLs in isolated CD4$^+$ T cells from PBMCs and LN cells at week 56 post-infection. Open symbols indicate viral DNA copies below the limit of detection. In **c**, **e** and **g**, plasma viral loads were measured longitudinally post-CD8$^+$ T-cell depletion (vertical dotted line). Horizontal dashed line indicates limit of detection of 26 SIV gag RNA copies per ml. In **d**, **f** and **h**, CAVLs from PBMCs were also measured longitudinally post-CD8$^+$ T-cell depletion. Grey box indicates a limit of detection range of 5–100 SIV gag DNA copies per 10^6 cells. Vertical dashed line indicates CD8$^+$ T-cell depletion at week 61. **i**, CAVLs in isolated CD4$^+$ T cells from PBMC, mesenteric LN, inguinal LN, axillary LN and spleen at necropsy. Open symbols indicate viral DNA copies below the limit of detection. **j**, Intact provirus copies in CD4$^+$ T cells from necropsy tissues (mesenteric LN, axillary LN, inguinal LN and spleen) of animals that received LRM, bNAb and cART at 72 h post-infection.

https://doi.org/10.1038/s41564-026-02444-x

The study presented here has potential limitations. Although we found no evidence of SHIV infection in any of the triple therapy-treated infants, it remains possible that deeper sampling of non-lymphoid tissues, such as bone marrow or the central nervous system, could have identified latent virus. Nevertheless, given the constraints of working with infant macaques, we elected to focus on lymphoid tissues since it is a major sanctuary site for latently infected cells. Although the synergy between LRM and bNAbs is promising for potential curative approaches, it may not be universally applicable, depending on the mechanism. For example, if the additive effect of LRM is due to

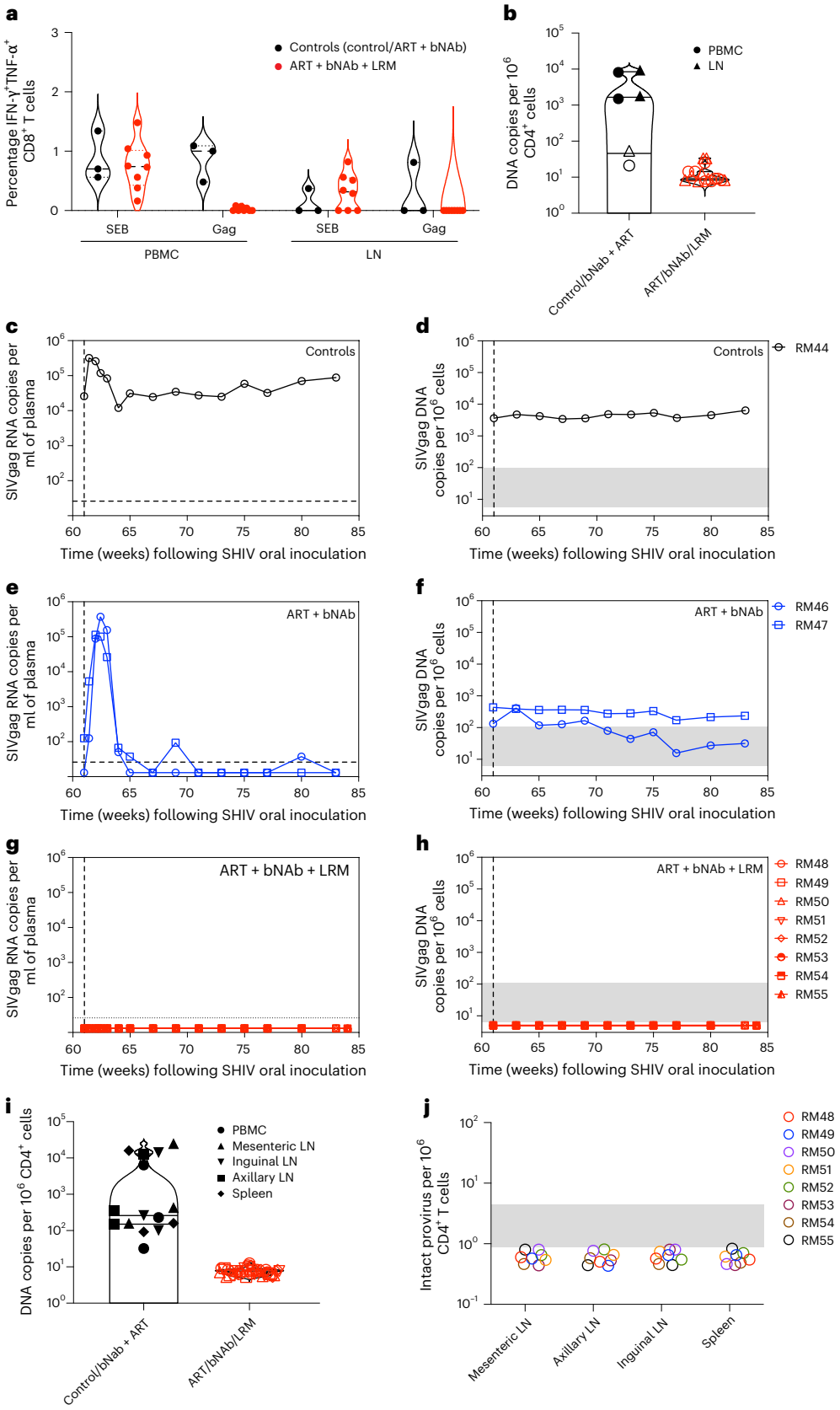

blockade of the CCR5 co-receptor, this approach may be ineffective against transmitted viruses utilizing the CXCR4 co-receptor. Finally, additional studies will be required to define whether triple therapy is also effective in the setting of adult HIV infection.

The discovery of an effective means of apparent viral elimination in the absence of adaptive immunity is remarkable. It suggests that despite ART, there is still ongoing replication and seeding of new viral foci during the maturation of the latent reservoir and that reducing this seeding could lead to an extinguished infection. These studies suggest an approach to cure that should be pursued, and, importantly, it may be possible to intervene later in infection and still disrupt the permanent reservoir. Both LRM and the bNAbs used in this study are currently in multiple human clinical trials with strong safety profiles[8,9,37], including in newborns[6,38], and thus, the potent antiviral combination of CCR5 blockade and bNAbs described here can readily be translated into clinical studies for the curative treatment of HIV in children.

Methods

Ethics statement

All experimental procedures were conducted at the Oregon National Primate Research Center (ONPRC) or the California National Primate Research Center (CNPRC), both of which are accredited by the Association for Assessment and Accreditation of Laboratory Animal Care International. Animal care adhered to the guidelines outlined in the 2011 *Guide for the Care and Use of Laboratory Animals* by the Institute for Laboratory Animal Research. All protocols were approved by the Institutional Animal Care and Use Committee at the University of California, Davis, or at Oregon Health & Science University. The Institutional Animal Care and Use Committee approval number is 23302.

Animals, virus infection and treatment groups

This study used outbred Indian origin rhesus macaques (*Macaca mulatta*) from the type D retrovirus-, SIV- and simian lymphocyte tropic virus type 1-free breeding colonies of the ONPRC and the CNPRC (Supplementary Table 2). Dams at both NPRCs lived in indoor–outdoor enclosures in group housing, and dams and sires (when there was a single male in the group) at the ONPRC were typed for MHC class I alleles. Newborns were screened by genetic testing for MHC class I alleles in the Primate Genetics Core at the ONPRC[39] and were excluded from assignment if they possessed MHC class I alleles, B*08 or B*17, as these alleles are associated with post-peak viral control. Infants were removed from dams within a few days of birth. Infant macaques of both sexes were raised in the nursery in pairs and orally infected with $SHIV_{SF162P3}$ at ~4 weeks of age by swallowing either without sedation (ONPRC) or while lightly sedated (CNPRC). Infants were infected using a potent, highly characterized, orally titrated virus stock grown in $CD4^+$-enriched rhesus splenocytes[19] that infects with two oral exposures on the same day. Contemporaneous controls were included in all experiments to demonstrate the potency of the viral stocks. Groups could not be balanced for sex owing to rolling assignments, as infants were accrued for the studies. Sex, age, and B*08 and B*17 MHC characteristics are listed in Supplementary Table 1. Daily ART was administered 72 h after virus exposure, with a duration of 28 weeks in most animals. Combination ART (cART) was administered in a once-daily subcutaneous injection (1 ml kg^{-1}) of tenofovir disoproxil fumarate (TDF; 5.1 mg kg^{-1}), emtricitabine (FTC; 40 mg kg^{-1}) and dolutegravir (DTG; 2.5 mg kg^{-1}) purchased from APIChem and formulated in-house in 15% KLEPTOSE HPB parenteral grade (Roquette) in sterile water, adjusted to pH 4.2, sterile filtered and stored at −20 °C. The cocktail was administered subcutaneously at 1 ml kg^{-1} each day for the indicated number of days[19]. Groups of animals were treated at 48 h or 72 h after oral exposure to SHIV with a bolus of two bNAbs, PGT121 and VRC07-523LS, 20 mg kg^{-1} each delivered subcutaneously. Six infants were similarly infected and treated weekly for 28 weeks with subcutaneous delivery of LRM at 50 mg kg^{-1}, followed by 10 mg kg^{-1} LRM alone, 6 with daily ART for 27 weeks plus LRM (8 weeks) or 2 with a 21-day course of daily ART + a bolus of bNAbs without LRM. Eight animals were treated with 27 weeks of daily ART, a bolus bNAb mixture (20 mg kg^{-1} each) and 8 weeks of LRM. After 27 weeks of daily ART, drug treatment was discontinued, and the kinetics of virus rebound (PVL and CAVL) was compared between the groups after ATI. Animals were monitored for clinical signs of disease by regular evaluation of body weight, peripheral LN size, appetite, behaviour and stool quality. Animals were euthanized under Institutional Animal Care and Use Committee guidelines using standard methods consistent with the recommendations of the American Veterinary Medical Association *Guidelines for the Euthanasia of Animals*. Sample sizes were calculated assuming a two-sided hypothesis test, with 80% power and alpha = 0.05. The number of macaques needed in each experimental group to be able to detect significant differences in PVL was determined. Experimental parameters were modelled using the virus stock $SHIV_{SF162P3}$ in *M. mulatta* newborns, $n = 6$. Week 2 data were used for the peak PVL in the controls (mean = 7.650 $\log_{10}$ and s.d. = 0.486 $\log_{10}$) and week 12 PVL for the set point (mean = 6.456 $\log_{10}$ and s.d. = 1.631 $\log_{10}$). The sample size needed in each group to see a halving of the set-point viral load (that is, a drop on average to 3.26 $\log_{10}$) was six. No data were excluded from the analyses. Animal care technicians, veterinarians and investigators assessing and documenting pathology were blinded to the animals' group assignments. Analyses of viral quantification in blood and tissues (plasma viral copies by droplet digital PCR, DNA in blood and tissues by droplet digital PCR, and IPDA on enriched CD4 cells by magnetic selection) were performed on samples that were coded to ensure that the laboratory performing the assays remained blinded. Animal assignment to study groups was done sequentially by birth date, rather than through randomization.

Blood and biopsy samples

Blood and tissue collection and processing. Peripheral blood was collected into EDTA-anticoagulant blood tubes before virus exposure on the day of challenge, on days 3, 7 and 14, and weekly thereafter. Blood tubes were centrifuged at 1,850 × *g* for 25 min with the brakes off to separate plasma from cells. The plasma supernatant was pipetted off, and aliquots were stored at −80 °C. The remaining blood fraction was resuspended in sterile phosphate-buffered saline (PBS) to double the original volume, and PBMCs were isolated by centrifugation in SepMate tubes (StemCell Technologies) or over Lymphocyte Separation Medium (Corning). For viral DNA detection by quantitative PCR as described below, 3×10^6 PBMCs were pelleted at ~20,000 × *g* in a benchtop microcentrifuge and frozen at −80 °C; any remaining PBMCs were cryopreserved in liquid nitrogen. Inguinal or axillary LNs were biopsied at various times post-exposure, and single-cell suspensions were made by crushing the tissue through a 100 µm strainer. LN cells were then frozen as pellets of 3×10^6 cells at −80 °C for viral quantitation, and any remaining cells were cryopreserved in liquid nitrogen. At necropsy, blood and a panel of 15 solid tissues were collected. From each solid tissue, 100 µg samples were excised and frozen at −80 °C in 2 ml tubes pre-filled with 1.4 mm zirconia beads (Spex SamplePrep) to facilitate tissue homogenization with a bead beater, nucleic acid extraction and viral DNA detection by quantitative PCR. For spleen and LNs at necropsy (mixed mesenteric LNs, axillary LNs, inguinal LNs and spleen), tissues were processed to make single-cell suspensions, which were enriched for $CD4^+$ T cells using magnetic beads, and then cryopreserved in liquid nitrogen for use in viral IPDAs.

Therapeutic antibodies and antiretroviral therapy

Human monoclonal IgG1 bNAb antibodies VRC07-523LS and PGT121[40,41] were produced at the Vaccine Research Center at NIH either in stable transfected CHO DG44 cell lines or by transient transfection in Expi293F cells (Thermo Fisher Scientific), respectively. Antibodies were affinity purified on Protein A columns to >95% purity. Antibodies were formulated in a cocktail and delivered subcutaneously around the

dorsal cervical and thoracic regions according to the dosing regimens described in the text. Clinical-grade LRM was provided by CytoDyn. All antibodies were tested for the presence of endotoxin.

In vivo CD8$^+$ cell depletion

For post-ATI depletion of CD8α$^+$ cells, macaques received four doses of anti-CD8α monoclonal antibody M-T807R1 (acquired through NHP Reagent Resource, AB_2716320). Macaques received 10 mg kg^{-1} subcutaneously on day 0 followed by 5 mg kg^{-1} intravenously on days 3, 7 and 10. Frequencies and absolute counts of CD8α$^+$ cell subsets were monitored as described previously[42].

Intracellular cytokine staining

SIV-specific CD8$^+$ T-cell responses were measured in PBMCs and LNs by flow cytometric intracellular cytokine staining, as described using mixes of sequential 15-mer peptides (11-amino-acid overlap) spanning the SIVmac239 Gag protein (sequence based on GenBank accession number M33262)[43,44]. Mononuclear cells were stimulated in the presence of antibodies anti-CD28 (CD28.2, purified 500 ng per test; Life Tech, CUST03277) and anti-CD49d (9F10, purified 500 ng per test; Life Tech, CUST03278) and then were incubated at 37 °C with peptide mixes and antibodies for 1 h, followed by an additional 8 h incubation in the presence of brefeldin A (5 μg ml^{-1}; BioLegend, 91850). Stimulation in the absence of peptides served as background control. Following the 9 h incubation, stimulated cells were stored at 4 °C until staining with combinations of fluorochrome-conjugated monoclonal antibodies including anti-CD3 (SP34-2; Alexa 700, BD Biosciences, 100 ng per test, 624041; and Pacific Blue, BD Biosciences, 624034, 100 ng per test), anti-CD4 (L200: BV786, Fisher Scientific, BDB56531, 220 ng per test; BV510, BD Biosciences, 624340, 220 ng per test; and BUV395, BD Biosciences, 624165, 220 ng per test), anti-CD8α (SK1: PerCP-eFluor 710, Life Tech, CUST04424, 8 ng per test), anti-TNF-α (MAB11: FITC, BioLegend, 624046, 20 ng per test; and PE, BioLegend, 96019, 20 ng per test), anti-IFN-γ (B27: APC, BioLegend, 96018, 80 ng per test) and anti-CD69 (FN50: PE, eBioscience, CUST01282, 50 ng per test; and PE/Dazzle 594, BioLegend, 93437, 50 ng per test). Stained samples were analysed on an LSR II or FACSymphony A5 flow cytometer (BD Biosciences). Data analysis was performed using the FlowJo software (BD Biosciences) with the gating strategy shown in Extended Data Fig. 6.

Measurements of LRM and ADAs in plasma and CCR5 RO on cells

Enzyme-linked immunosorbent assay was used to detect LRM levels in plasma samples[33]. Plates were coated with 1.5 μg ml^{-1} PA22 (CytoDyn) in carbonate–bicarbonate buffer (Thermo Fisher) overnight at 4 °C, then washed three times with PBS-T (PBS with 0.1% Tween 20), and blocked for at least 2 h at room temperature with a blocking buffer (PBS with 0.4% Tween 20 and 10% bovine serum albumin; Fisher Scientific). A standard curve was generated with serial dilutions of LRM, and samples were plated onto blocked plates and incubated for 30 min at room temperature. Plates were washed three times with PBS containing 0.5 M NaCl and then incubated with 20,000-fold diluted mouse anti-human IgG4 pFc′-horseradish peroxidase (Southern Biotech) in a blocking buffer for 30 min at room temperature. Finally, plates were washed three times with PBS-T, and 3,3′,5,5′-tetramethylbenzidine substrate (Southern Biotech) was added to develop the plates for 2 min, after which 1 N H_2SO_4 was added to stop the reaction. Developed plates were read on the Synergy HTX Multi-Mode Microplate Reader (BioTek) using the Gen5 v3.10 software to read two absorbance wavelengths: 650 nm for the developing reaction and 450 nm for the developed reaction. The plasma concentration of each sample (μg ml^{-1}) was determined using the generated standard curve, with an assay limit of detection of 0.0226 μg ml^{-1}.

LRM ADAs were measured via enzyme-linked immunosorbent assay. Costar 96-well Half-Area Assay Plates (Corning) were coated with human LRM (2 mg ml^{-1}, CytoDyn) diluted in carbonate–bicarbonate buffer (Thermo Fisher) overnight at 4 °C. Plates were then washed three times with PBS-T and blocked with a blocking buffer for at least 2 h at RT. Plates were then washed three times with PBS-T. Heat-inactivated plasma samples were serially diluted in a blocking buffer across six steps and plated onto blocked plates in duplicates for 30 min at RT. After this incubation step, plates were washed three times with 0.5 M NaCl in PBS and incubated with 20,000-fold diluted secondary antibody, mouse anti-human IgG4 pFc′-HRP (HP6025, Invitrogen, MA1-34437), in a blocking buffer. Plates were incubated at RT for 30 min, with the remaining steps following the quantification enzyme-linked immunosorbent assay described above. ADA titres were defined as the ID50 (OD 450/65).

CCR5 RO was measured by flow cytometry. For each sample assayed, three staining tubes were used: tube 1, a negative control tube without LRM secondary detection antibody and without LRM-Pacific Blue (LRM-PB); tube 2, a tube detecting cell-bound LRM present in vivo via anti-human IgG4-FITC (HP-6025, Sigma, F9890, 3:100) and unoccupied CCR5 receptors present in vivo by LRM-PB staining; and tube 3, a positive control tube where cells were saturated ex vivo by addition of 5 mg ml^{-1} human LRM before LRM secondary detection and LRM-PB staining. Anti-human IgG4-FITC was used as the secondary antibody for LRM detection. PBS-reconstituted blood was thoroughly washed with 1× PBS before aliquoting ~100 ml of blood per staining tube. The staining protocol consisted of washing all tubes once with 1× PBS, incubating tube 3 with a saturating concentration (5 mg ml^{-1}) of human LRM for 30 min, washing all tubes once with 1× PBS, incubating tubes 2 and 3 with the anti-human IgG4-FITC antibody for 30 min, washing all tubes once with FACS buffer (1× PBS with 10% bovine growth serum) and three times with 1× PBS, and finally incubating all tubes with surface mastermix and tubes 2 and 3 only with LRM-PB (surface mastermix and LRM-PB staining in the same incubation). Surface mastermix included Live/Dead amine-reactive dye (near-IR, Invitrogen, L-34976) and the following antibodies: anti-CD3 (SP34-2: Alexa 700, BD Biosciences, 100 ng per test, 624041), anti-CD4 (L200: BUV395, BD Biosciences, 624165, 220 ng per test), CD8α (SK1: BUV737, BD Biosciences, 200 ng per test, 612754), anti-CD45 (D058-1283: PE-Cy7, BD Biosciences, 200 ng per test) and anti-CCR5 (J418F1: APC, BioLegend, 359122, 100 ng per test). After the final staining incubation, blood RO samples were treated with 1× FACS Lyse for 8 min and then pelleted and washed three times with FACS buffer. All samples were collected on a BD LSR II or BD A5 Symphony flow cytometer and analysed using FlowJo (BD). Gating on live CCR5$^+$CD4$^+$ T cells was performed by progressively gating on singlet, CD45 hi/mid, live, CD3$^+$, CD4$^+$ and CCR5$^+$ events (Extended Data Fig. 7). Calculations were performed as follows, where % represents frequency within the live CCR5$^+$CD4$^+$ T-cell gate:

CCR5 RO Equation 1 (saturation)

$$\%\mathrm{RO} = (\%\mathrm{IgG4} + \mathrm{in\ tube\ 2}/\%\mathrm{IgG4} + \mathrm{in\ tube\ 3}) \times 100\%$$

CCR5 RO Equation 2 (leron-PB)

$$\%\mathrm{RO} = (\%\mathrm{IgG4} + \mathrm{in\ tube\ 2}/[\%\mathrm{IgG4} + \mathrm{in\ tube\ 2} + (\%\mathrm{leron} - \mathrm{PB} + \mathrm{in\ tube\ 2} - \%\mathrm{leron} - \mathrm{PB} + \mathrm{in\ tube\ 3})]) \times 100\%$$

The two CCR5 RO equations yielded similar results, and thus, equation 1 (saturation) is shown in all CCR5 RO graphs.

Measurements of plasma viral loads, CAVLs and intact proviral DNA

Plasma SIV RNA levels were determined using an SIV Gag-targeted quantitative RT-PCR format assay, with six replicate reactions analysed per extracted sample for an assay threshold of 26–50 SIV RNA copies per ml, depending on the input volume of plasma, as previously described[19] using the following primers: SGAG21

forward (5′-GTCTGCGTCATPTGGTGCATTC-3′), SGAG22 reverse (5′-CACTAGKTGTCTCTGCACTATPTGTTTTG-3′) and pSGAG23 probe (5′-[FAM]-CTTCPTCAGTKTGTTTCACTTTCTCTTCTGCG-[BHQ1]-3′).

Quantitative assessment of SHIV DNA in cells and tissues was performed using SIV Gag-targeted, nested quantitative hybrid real-time/digital RT-PCR and PCR assays, as previously described[19] using the following primers: primers for pre-amplification of viral DNA were SIVnestF01 (GATTTGGATTAGCAGAAAGCCTGTTG) and SIVnestR01 (GTTGGTCTACTTGTTTTTGGCATAGTTTC), and primers for quantitative PCR were SGAG21 forward, SGAG22 reverse and pSGAG23, as described above. SIV Gag-DNA copy numbers were normalized based on quantitation of a single-copy rhesus genomic DNA sequence from the CCR5 locus from the same specimen, as described, to allow normalization of SIV DNA copy numbers per 10^6 diploid genome cell equivalents. Ten replicate reactions were performed with aliquots of extracted DNA from each sample, with two additional spiked internal control reactions performed with each sample to assess potential reaction inhibition. Samples that did not yield any positive results across the replicate reactions were reported as a value of 'less than' the value that would apply for 1 positive reaction out of 10. Threshold sensitivities for individual specimens varied as a function of the number of cells or the amount of tissue available and analysed. Plasma and cell-associated viral quantification was performed by the Molecular Virology Core at the ONPRC using coded samples. IPDAs were performed as previously described in the Siliciano Laboratory at The Johns Hopkins University[12]. In brief, DNA from isolated $CD4^+$ T cells was subjected to droplet digital PCR to quantify intact SHIV genomes (targets in pol and env), host gene *rpp30* (for input cell number quantitation and DNA shearing correction) and 2-LTR circles (for background subtraction of unintegrated viral DNA). For $CD4^+$ CAVL and IPDAs, $CD4^+$ cells were isolated from samples before assays using positive selection (nonhuman primate CD4 microbeads, Miltenyi Biotec).

RNAscope in situ hybridization with immunofluorescent staining

Formalin-fixed paraffin-embedded lymphoid 5-µm-thick tissue sections were processed for simultaneous detection of SHIV RNA using RNAscope and immunofluorescent staining for CD3 and DAPI. Slides were baked at 60 °C for 1 h, deparaffinized in xylene (two washes, 5 min each) and placed in 100% ethanol (two washes, 3 min each), followed by rinsing three times in distilled water (diH_2O). Antigen retrieval was conducted using a Decloaking Chamber (Biocare Medical, catalogue number DCARC001) in 1× AR9 buffer (Akoya Biosciences, catalogue number AR900250ML) at 110 °C for 15 min. Slides were rinsed and placed in diH_2O to prevent drying and protect from light exposure. To reduce autofluorescence, slides were incubated in a photobleaching solution (PBS, 30% hydrogen peroxide and 5 M sodium hydroxide) for 45 min under a light source. Slides were then rinsed twice in diH_2O for 2 min. The SIVmac239 RNA probe (ACD, catalogue number 312811) was diluted 1:2 in a probe diluent. Probe hybridization was performed on the Leica BOND system. Amplification steps were conducted according to the manufacturer's instructions using the RNAscope 2.5 HD Reagent Kit-BROWN (ACD, catalogue number 322300). Immunofluorescent staining was performed as follows: the slides were incubated for 2 h at RT with primary rabbit anti-CD3 antibody (Thermo Scientific, catalogue number RM-9107-S). Slides were washed in 1× TBS–Tween 20 (TBS-T) for 5 min. The secondary antibody (Alexa Fluor 647-conjugated goat anti-rabbit IgG, Invitrogen, catalogue number A-21244) was applied for 1 h at RT in a 0.25% casein solution. Nuclei were counterstained with DAPI (1:10,000 dilution in PBS) for 10 min. Slides were mounted with ProLong Diamond Antifade Mountant (Invitrogen, P36970) and coverslipped. Slides were scanned using the Axio Scan.Z1 slide scanner. Images were saved in the standard pyramid-tiled TIFF format with JPEG compression. Image analysis was performed using the HALO platform (v.4.1; Indica Labs) to quantify viral RNA by area (µm^2) in stained tissue sections. The Area Quantification FL v2.3.4 (Indica Labs) module within the software was used for analysis.

Measurements of plasma bNAb concentrations

Plasma bNAb levels were quantified using plates coated with either RSC3 (ref. 45) for specific detection of VRC07-523LS or ST0A9 (ref. 46) for specific detection of PGT121. Costar Half-Area High Binding (Corning) plates were coated overnight at 4 °C with 200 ng per well of ST0A9 or 100 ng per well of RSC3 in carbonate–bicarbonate buffer (Thermo Fisher), washed one time with wash buffer (PBS with 0.1% Triton X-100) and blocked with PBS with 1% normal goat serum and 5% nonfat dry milk for 1 h at RT. Serial dilutions of all samples, each bNAb (for standard curves) and positive and negative controls were included on each plate. Plasma was incubated for 1 h at RT, followed by three washes. Bound bNAbs were probed with a horseradish peroxidase-labelled goat anti-human IgG (1:5,000 dilution; Jackson Laboratory) for 1 h at RT. The plate was washed five times, and 3,3′,5,5′-tetramethylbenzidine (Surmodics) substrate was added. Once colour was developed, a stopping buffer (1 N H_2SO_4) was added, and the optical density was read at 450 nm. The GraphPad Prism and Microsoft Office software were used to plot standard curves and calculate bNAb concentrations.

Measurement of anti-SF162 gp140 trimer antibodies

Costar Half Area High Binding (Corning) plates were coated overnight at 4 °C with 0.5 µg ml^{-1} of SF162 gp140 trimer (provided by Noah Sather) in carbonate–bicarbonate buffer (Thermo Fisher), washed one time with wash buffer (PBS with 0.1% Triton X-100) and blocked with PBS with 1% normal goat serum and 5% nonfat dry milk for 1 h at RT. Serial dilutions of all heat-inactivated plasma samples and VRC07-523LS as a positive control were plated in duplicate and incubated for 1 h at RT, followed by three washes. Bound antibodies were probed with a horseradish peroxidase-labelled goat anti-human IgG (1:5,000 dilution; Jackson Laboratory) for 1 h at RT. The plate was washed five times, and 3,3′,5,5′-tetramethylbenzidine (Surmodics) substrate was added. Once colour was developed, a stopping buffer (1 N H_2SO_4) was added, and the optical density at 450 nm was read. GraphPad Prism was used to plot curves.

Pathology

At necropsy, tissues and fluids were collected as fresh, frozen or fixed in 10% neutral buffered formalin. Tissues for microscopic evaluation were routinely processed, sectioned at 5 µm and stained with haematoxylin and eosin. Gross and microscopic post-mortem evaluations were performed by veterinary pathologists blinded to group assignment. Diagnosis of opportunistic infections was performed as previously described[19].

Reporting summary

Further information on research design is available in the Nature Portfolio Reporting Summary linked to this article.

Data availability

All datasets generated and analysed during this study are included in this published article, its Supplementary Information files and as source data. Source data are provided with this paper.

References

1. Siliciano, J. M. & Siliciano, R. F. The remarkable stability of the latent reservoir for HIV-1 in resting memory $CD4^+$ T cells. *J. Infect. Dis.* **212**, 1345–1347 (2015).
2. Berendam, S. J. et al. Pediatric HIV: the potential of immune therapeutics to achieve viral remission and functional cure. *Curr. HIV/AIDS Rep.* **17**, 237–248 (2020).

3. Mallik, I., Henderson, M., Fidler, S. & Foster, C. Aging of adult lifetime survivors with perinatal HIV. *Curr. Opin. HIV AIDS* **20**, 379–387 (2025).
4. Pegu, A., Hessell, A. J., Mascola, J. R. & Haigwood, N. L. Use of broadly neutralizing antibodies for HIV-1 prevention. *Immunol. Rev.* **275**, 296–312 (2017).
5. Corey, L. et al. Two randomized trials of neutralizing antibodies to prevent HIV-1 acquisition. *N. Engl. J. Med.* **384**, 1003–1014 (2021).
6. Shapiro, R. L., Masheto, G. & Ajibola, G. Use of broadly neutralizing antibodies in pediatric HIV for treatment and remission. *Curr. Opin. HIV AIDS* **20**, 279–286 (2025).
7. Bar-On, Y. et al. Safety and antiviral activity of combination HIV-1 broadly neutralizing antibodies in viremic individuals. *Nat. Med.* **24**, 1701–1707 (2018).
8. Julg, B. et al. Safety and antiviral effect of a triple combination of HIV-1 broadly neutralizing antibodies: a phase 1/2a trial. *Nat. Med.* **30**, 3534–3543 (2024).
9. Gathe, J. C. et al. Leronlimab Treatment for Multidrug-Resistant HIV-1 (OPTIMIZE): a randomized, double-blind, placebo-controlled trial. *JAIDS J. Acquir. Immune Defic. Syndr.* **99**, 185–194 (2025).
10. Yang, B. et al. Clinical characteristics and outcomes of coronavirus disease 2019 patients who received compassionate-use leronlimab. *Clin. Infect. Dis.* https://doi.org/10.1093/cid/ciaa1583 (2020).
11. Chang, X. L. et al. Antibody-based CCR5 blockade protects macaques from mucosal SHIV transmission. *Nat. Commun.* **12**, 3343 (2021).
12. Bender, A. M. et al. The landscape of persistent viral genomes in ART-treated SIV, SHIV, and HIV-2 infections. *Cell Host Microbe* **26**, 73–85 e4 (2019).
13. Whitney, J. B. et al. Rapid seeding of the viral reservoir prior to SIV viraemia in rhesus monkeys. *Nature* **512**, 74–77 (2014).
14. Keele, B. F. et al. Early antiretroviral therapy in SIV-infected rhesus macaques reveals a multiphasic, saturable dynamic accumulation of the rebound competent viral reservoir. *PLoS Pathog.* **20**, e1012135 (2024).
15. Whitney, J. B. et al. Prevention of SIVmac251 reservoir seeding in rhesus monkeys by early antiretroviral therapy. *Nat. Commun.* **9**, 5429 (2018).
16. Pitchai, F. N. N. et al. Engineered deletions of HIV replicate conditionally to reduce disease in nonhuman primates. *Science* **385**, eadn5866 (2024).
17. Jayaraman, P. et al. Evidence for persistent, occult infection in neonatal macaques following perinatal transmission of simian-human immunodeficiency virus SF162P3. *J. Virol.* **81**, 822–834 (2007).
18. Shapiro, M. B. et al. Immune perturbation following SHIV infection is greater in newborn macaques than in infants. *JCI Insight* **9**, e144448 (2024).
19. Shapiro, M. B. et al. Single-dose bNAb cocktail or abbreviated ART post-exposure regimens achieve tight SHIV control without adaptive immunity. *Nat. Commun.* **11**, 70 (2020).
20. van Rompay, K. K. A. et al. Early short-term 9-[2-(*R*)-(phosphonomethoxy)propyl]adenine treatment favorably alters the subsequent disease course in simian immunodeficiency virus-infected newborn rhesus macaques. *J. Virol.* **73**, 2947–2955 (1999).
21. Hessell, A. J. et al. Early short-term treatment with neutralizing human monoclonal antibodies halts SHIV infection in infant macaques. *Nat. Med.* **22**, 362–368 (2016).
22. Stahl-Hennig, C. et al. Rapid infection of oral mucosal-associated lymphoid tissue with simian immunodeficiency virus. *Science* **285**, 1261–1265 (1999).
23. Milush, J. M. et al. Rapid dissemination of SIV following oral inoculation. *AIDS* **18**, 2371–2380 (2004).
24. Hessell, A. J. et al. Achieving potent autologous neutralizing antibody responses against tier 2 HIV-1 viruses by strategic selection of envelope immunogens. *J. Immunol.* **196**, 3064–3078 (2016).
25. John, G. C. et al. Correlates of mother-to-child human immunodeficiency virus type 1 (HIV-1) transmission: association with maternal plasma HIV-1 RNA load, genital HIV-1 DNA shedding, and breast infections. *J. Infect. Dis.* **183**, 206–212 (2001).
26. Persaud, D. et al. HIV-1 reservoir size after neonatal antiretroviral therapy and the potential to evaluate antiretroviral-therapy-free remission (IMPAACT P1115): a phase 1/2 proof-of-concept study. *Lancet HIV* **11**, e20–e30 (2024).
27. Cunningham, C. K. et al. Safety, tolerability, and pharmacokinetics of long-acting broadly neutralizing HIV-1 monoclonal antibody VRC07-523LS in newborn infants exposed to HIV-1. *J. Pediatr. Infect. Dis. Soc.* **14**, piaf002 (2025).
28. Chang, X. L. et al. Suppression of human and simian immunodeficiency virus replication with the CCR5-specific antibody leronlimab in two species. *PLoS Pathog.* **18**, e1010396 (2022).
29. Ardeshir, A. et al. Determinants of successful AAV-vectored delivery of HIV-1 bNAbs in early life. *Nature* **645**, 1–9 (2025).
30. Wu, H. L. et al. Adeno-associated virus gene therapy-mediated CCR5 blockade suppresses virus replication long term in SHIV-infected macaques. *Sci. Transl. Med.* **18**, eadw1976 (2026).
31. Keele, B. F. et al. Initial sites of SIV rebound after antiretroviral treatment cessation in rhesus macaques. *Nat. Microbiol.* **11**, 648–663 (2026).
32. Rompay, K. K. V. et al. A vaccine against CCR5 protects a subset of macaques upon intravaginal challenge with simian immunodeficiency virus SIVmac251. *J. Virol.* **88**, 2011–2024 (2014).
33. Chang, X. L. et al. CCR5 receptor occupancy analysis reveals increased peripheral blood $CCR5^{+}CD4^{+}$ T cells following treatment with the anti-CCR5 antibody leronlimab. *Front. Immunol.* **12**, 794638 (2021).
34. Moy, R. H. et al. Clinical and immunologic impact of CCR5 blockade in graft-versus-host disease prophylaxis. *Blood* **129**, 906–916 (2017).
35. Reshef, R. et al. Blockade of lymphocyte chemotaxis in visceral graft-versus-host disease. *N. Engl. J. Med.* **367**, 135–145 (2012).
36. Huang, Y. et al. Engineered bispecific antibodies with exquisite HIV-1-neutralizing activity. *Cell* **165**, 1621–1631 (2016).
37. Seethamraju, H. et al. A randomized placebo-controlled trial of leronlimab in mild-to-moderate COVID-19. *Clin. Ther.* **46**, 891–899 (2024).
38. Cunningham, C. K. et al. Safety, tolerability, and pharmacokinetics of the broadly neutralizing human immunodeficiency virus (HIV)-1 monoclonal antibody VRC01 in HIV-exposed newborn infants. *J. Infect. Dis.* **222**, 628–636 (2020).
39. Karl, J. A., Wiseman, R. W. & O'Connor, D. H. Cost-effective sequence-based nonhuman primate MHC class I genotyping from RNA. *Methods* **49**, 11–17 (2009).
40. Rudicell, R. S. et al. Enhanced potency of a broadly neutralizing HIV-1 antibody in vitro improves protection against lentiviral infection in vivo. *J. Virol.* **88**, 12669–12682 (2014).
41. Walker, L. M. et al. Broad neutralization coverage of HIV by multiple highly potent antibodies. *Nature* **477**, 466–470 (2011).
42. Wu, H. L. et al. Allogeneic immunity clears latent virus following allogeneic stem cell transplantation in SIV-infected ART-suppressed macaques. *Immunity* **56**, 1649–1663.e5 (2023).
43. Malouli, D. et al. Cytomegalovirus vaccine vector-induced effector memory $CD4^{+}$ T cells protect cynomolgus macaques from lethal aerosolized heterologous avian influenza challenge. *Nat. Commun.* **15**, 6007 (2024).

44. Malouli, D. et al. Cytomegalovirus-vaccine-induced unconventional T cell priming and control of SIV replication is conserved between primate species. *Cell Host Microbe* **30**, 1207–1218.e7 (2022).
45. Lynch, R. M. et al. The development of CD4 binding site antibodies during HIV-1 infection. *J. Virol.* **86**, 7588–7595 (2012).
46. Zhou, T. et al. Transplanting supersites of HIV-1 vulnerability. *PLoS ONE* **9**, e99881 (2014).

Acknowledgements

We thank the staff of Research Services, Pathology and Clinical Laboratories of the California National Primate Research Center, and the staff of the Clinical Medicine, Pathology Services, and Behavioral Services at the Oregon National Primate Research Center for expert technical assistance and animal care. This research was supported by the Primate Genetics, Molecular Virology and Flow Cytometry Cores of the Oregon National Primate Research Center. We thank J. Mitchell for helpful scientific discussions and suggestions for the project. We thank K. Carlton and the staff of the Vaccine Production Program, NIH Vaccine Research Center, for the manufacture of VRC07-523LS, and X.J. Chen and C. Liu of the Virology Core Laboratory at the NIH Vaccine Research Center for the manufacture of PGT121. The funders had no role in the study design, data collection and analysis, decision to publish or preparation of the manuscript.

Author contributions

J.B.S. contributed to funding, conceptualization, statistical analyses and validation, and co-wrote the first draft with N.L.H., reviewing and editing. T.O., S.P., P.B., C.P., M.C.H., J.R., A.F., A.M., J.K.W., J.L.U., R.M.W. and S.V. contributed to project management, experimental design and data analysis. G.W. contributed to project management, supervision, data analyses and figure design. H.S. contributed to veterinary oversight, clinical monitoring and analyses, and validation. A.D.L. and G.P. contributed to pathology and expert data analyses. S.O., A.B.-A., B.S. and R.B. contributed to project management, supervision, sample collection and validation. J.R.M. and A.P. contributed to conceptualization, resources, validation, writing, reviewing and editing. E.J.F., J.D.S. and R.F.S. contributed to conceptualization, experimental design, validation, reviewing and editing. S.G.H. contributed to experimental design, data analysis, validation, supervision and reviewing. K.K.A.V.R. contributed to conceptualization, data analyses, supervision, validation, writing, reviewing and editing. A.J.H. contributed to conceptualization, data analysis, supervision, validation, reviewing and editing. N.L.H. contributed to funding, conceptualization, data analysis, statistical analyses and validation, and co-wrote the first draft with J.B.S., reviewing and editing.

Funding

Funding for this work was supported by grants from the US Health and Human Services NIH HD080459 (N.L.H.), R01AI154559 (N.L.H.), R01AI166969 (J.B.S.), R01AI129703 (J.B.S.), P51 OD011092 (ONPRC), P51 OD011107 (CNPRC), U42 OD010426 (ONPRC), K01 OD036063 (R.M.W.) 5U42OD010990 (K.K.A.V.R.), R01AI200511 (J.B.S.) and R37AI189285 (J.B.S.).

Competing interests

S.G.H. and J.B.S. have a significant financial interest in CytoDyn, a company that may have a financial interest in the results of this research and technology. J.B.S. also serves on the scientific advisory board of CytoDyn. This potential individual conflict of interest has been reviewed and managed by Oregon Health & Science University. The other authors declare no competing interests.

Additional information

Extended data is available for this paper at https://doi.org/10.1038/s41564-026-02444-x.

Supplementary information The online version contains supplementary material available at https://doi.org/10.1038/s41564-026-02444-x.

Correspondence and requests for materials should be addressed to Jonah B. Sacha or Nancy L. Haigwood.

Peer review information *Nature Microbiology* thanks Michael Betts, Roger Le Grand and the other, anonymous, reviewer(s) for their contribution to the peer review of this work. Peer reviewer reports are available.

Reprints and permissions information is available at www.nature.com/reprints.

Publisher's note Springer Nature remains neutral with regard to jurisdictional claims in published maps and institutional affiliations.

[1]Oregon National Primate Research Center, Oregon Health & Science University, Portland, OR, USA. [2]Vaccine & Gene Therapy Institute, Oregon Health & Science University, Portland, OR, USA. [3]California National Primate Research Center, Microbiology and Immunology, University of California, Davis, CA, USA. [4]Vaccine Research Center, National Institute of Allergy and Infectious Diseases, National Institutes of Health, Bethesda, MD, USA. [5]Department of Medicine, The Johns Hopkins University School of Medicine, Baltimore, MD, USA. [6]Howard Hughes Medical Institute, The Johns Hopkins University School of Medicine, Baltimore, MD, USA. [7]Department of Pathology, Microbiology and Immunology, University of California, Davis, CA, USA. [8]Present address: ModeX Therapeutics, Weston, MA, USA. ✉e-mail: sacha@ohsu.edu; haigwoon@ohsu.edu

https://doi.org/10.1038/s41564-026-02444-x

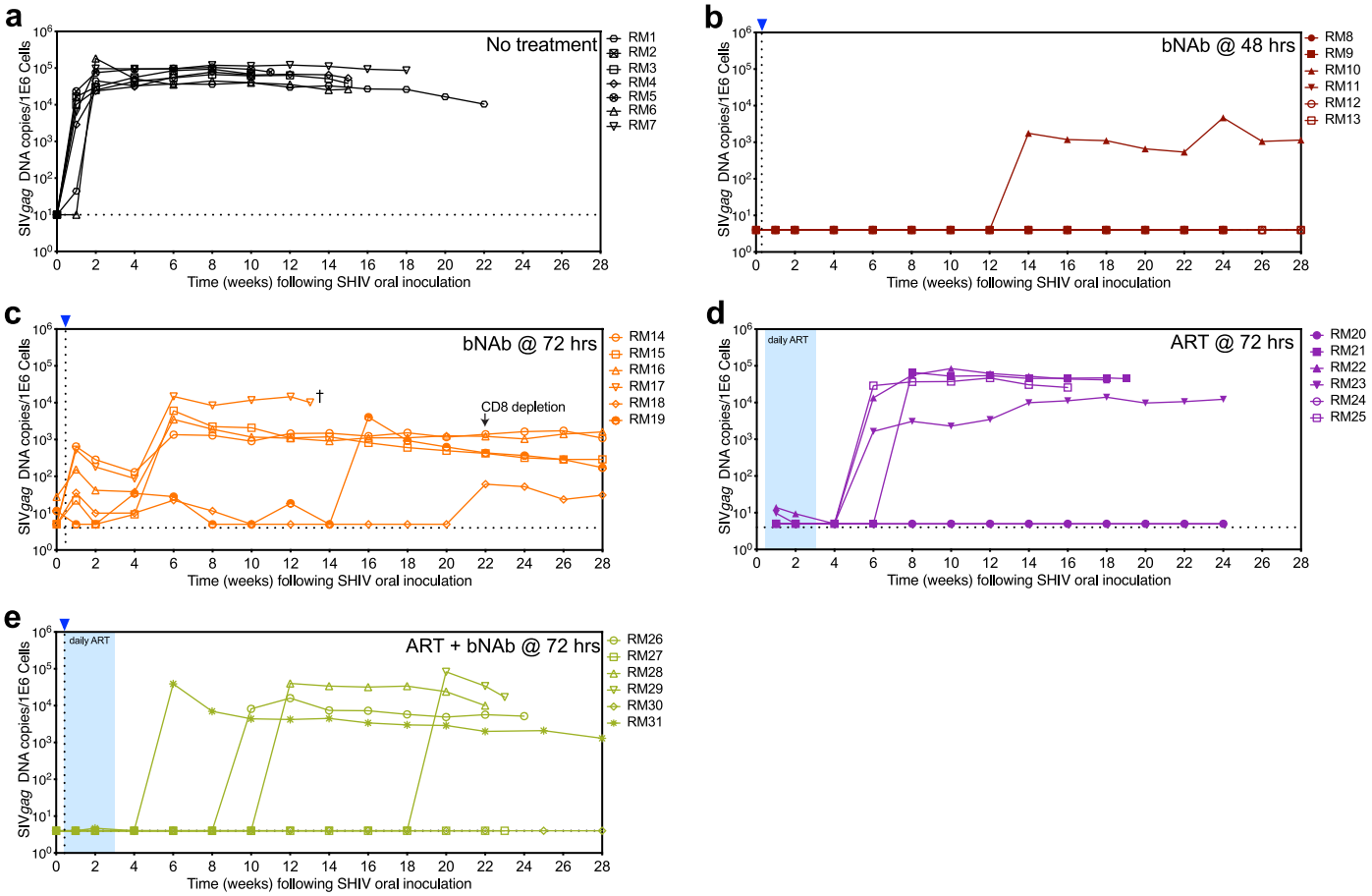

Extended Data Fig. 1 | Cell-associated viral loads after early bNAb and cART treatment in infants. Cell-associated viral loads were measured longitudinally. **a** No treatment controls. **b** bNab administration at 48 h. **c** bNAb administration at 72 h. **d** cART administration at 72 h for 21 days. **e** bNAb administration at 72 h and cART administration at 72 h for 21 days. Horizontal dashed line indicates a limit of detection of 8 SIV gag DNA copies/10^6 cells. Vertical dashed line and blue arrow indicate bNAb administration. Blue box indicates time on cART. Symbols for individual animals are defined in the legends.

https://doi.org/10.1038/s41564-026-02444-x

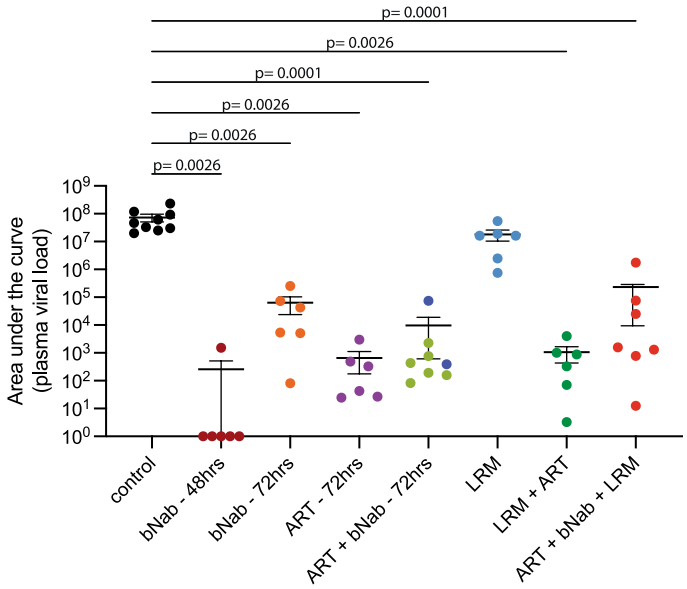

Extended Data Fig. 2 | Acute plasma viral load area under the curve. Area under the curve of acute plasma viral loads through week 3 post-infection. Values for individual animals are shown by group and labeled on the X axis. P values were calculated using Two-way ANOVA, mixed-effect analysis with Tukey's multiple comparison test.

https://doi.org/10.1038/s41564-026-02444-x

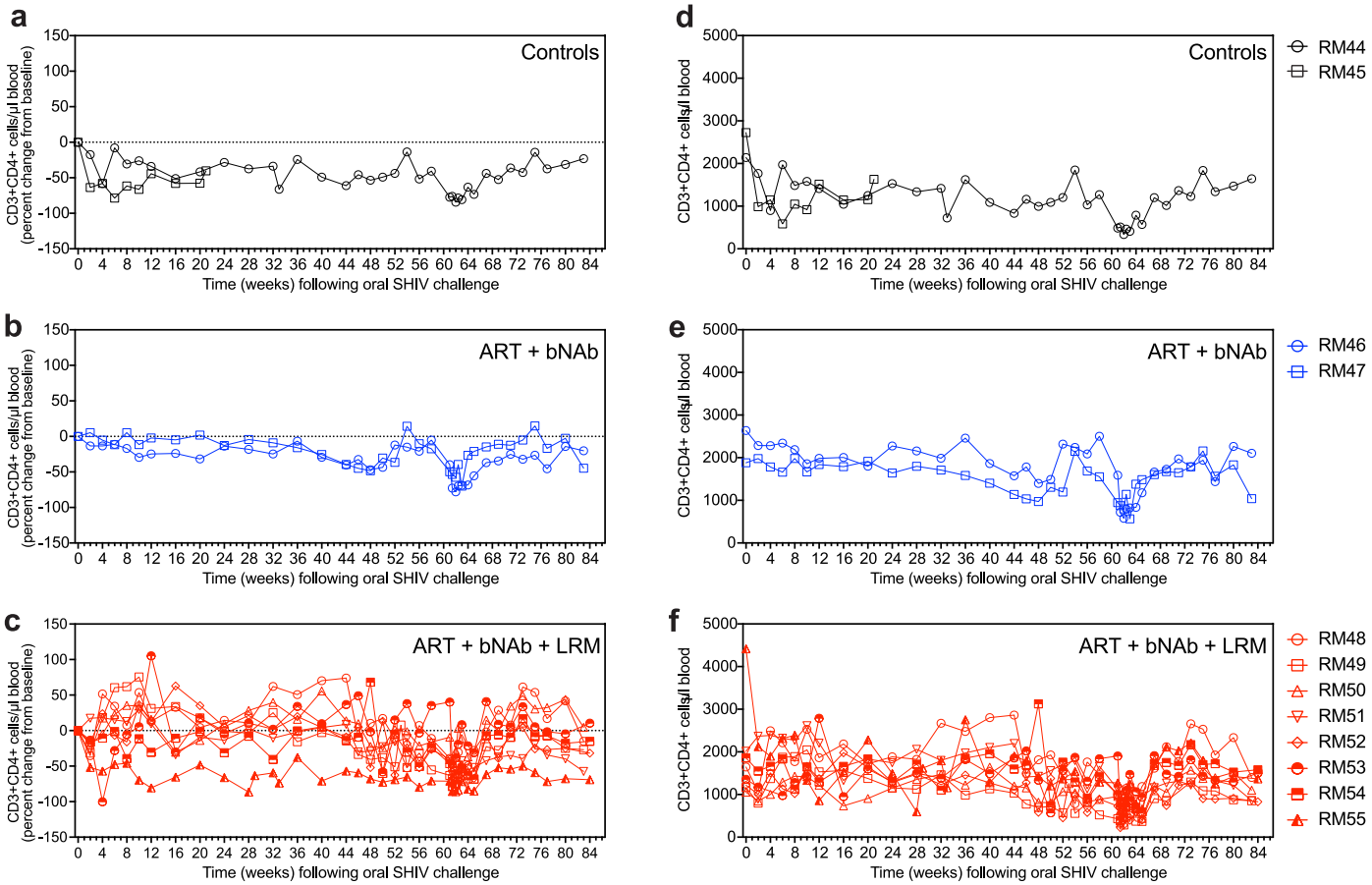

Extended Data Fig. 3 | CD4 T cell counts in macaques in the triple therapy experiment. Longitudinal absolute CD4 + T cell counts in blood as a percent change from baseline (**a**–**c**) and per µl of blood (**d**–**f**). Individual animals are defined in the legends. See Extended Data Fig. 8 for gating strategy.

https://doi.org/10.1038/s41564-026-02444-x

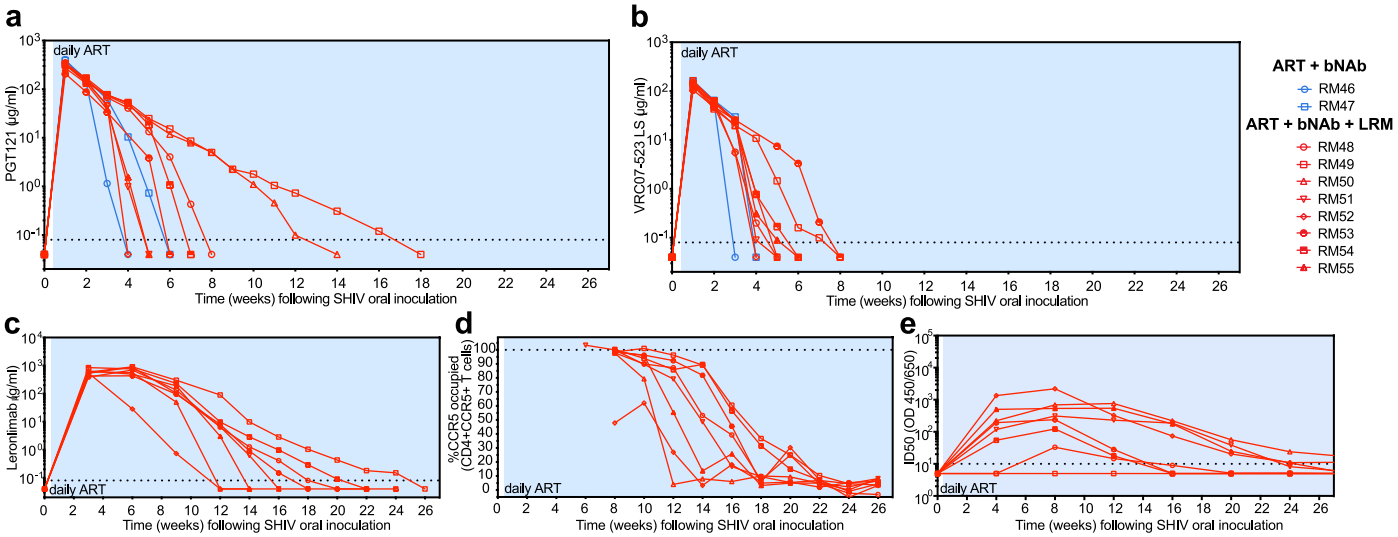

Extended Data Fig. 4 | Plasma concentrations of bNAbs and Leronlimab and Leronlimab receptor occupancy and anti-drug antibodies. a PGT121 plasma concentrations. **b** VRC07-523LS plasma concentrations. **c** Longitudinal Leronlimab plasma concentrations. **d** Longitudinal CCR5 receptor occupancy (RO) of blood CD4 + T cells. **e** Longitudinal ID50 of anti-drug antibodies (ADA) against Leronlimab in plasma. Horizontal dashed lines indicate limit of detection. Individual animals are defined in the legend.

https://doi.org/10.1038/s41564-026-02444-x

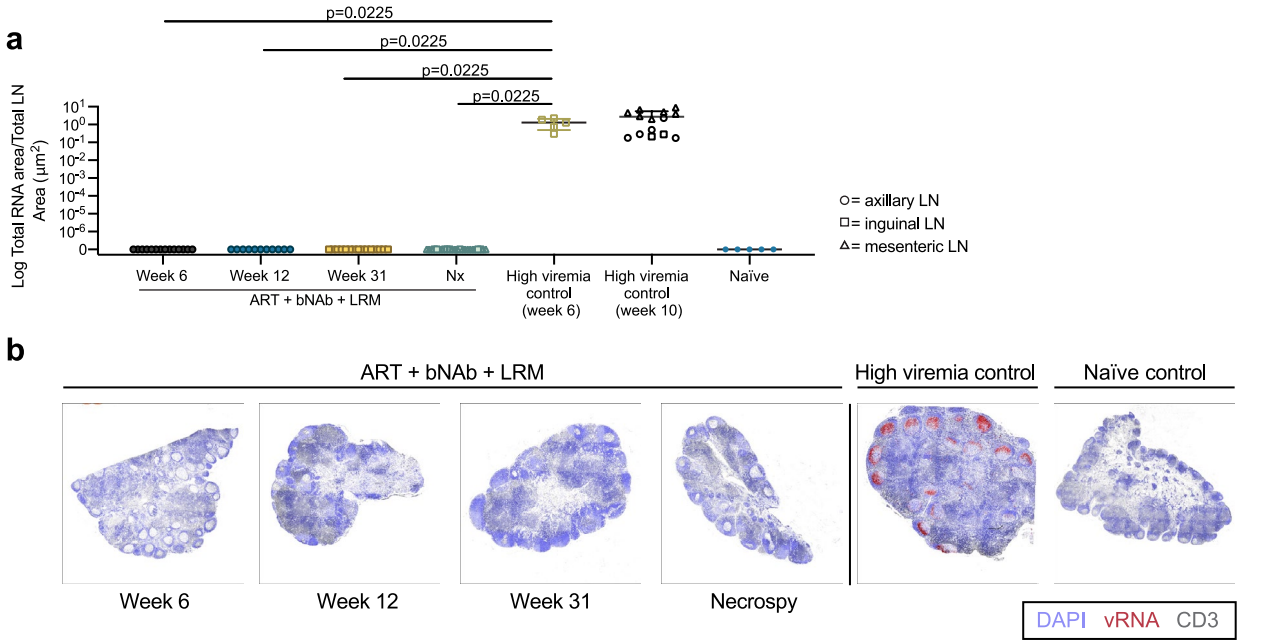

Extended Data Fig. 5 | *In situ* hybridization and immunofluorescent staining of lymph nodes. a HALO quantification of SHIV RNA (log total RNA area/total LN area, µm²) in lymph node sections from treated and control animals. Each data point represents an individual lymph node: circles indicate axillary, squares indicate inguinal, and triangles indicate mesenteric lymph nodes at various weeks post infection or necropsy. Horizontal lines denote group medians. $p < 0.05$ compared to week 6 high-viremia controls. **b** Representative whole lymph node images from each group are shown, blue = DAPI, red = vRNA, grey = CD3 positive cells. RNAscope staining was performed once on 1–2 lymph nodes collected from each animal at each designated time point.

https://doi.org/10.1038/s41564-026-02444-x

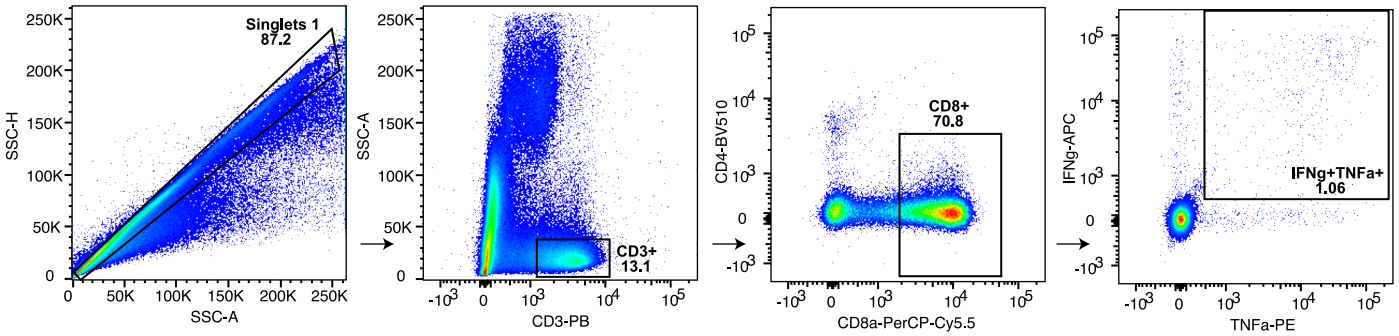

Extended Data Fig. 6 | Representative gating strategy for intracellular cytokine stain. Events were gated for IFNγ + TNFα + CD8 + T cells by progressively gating on singlet, CD3+, CD8+, IFNγ + TNFα + events.

https://doi.org/10.1038/s41564-026-02444-x

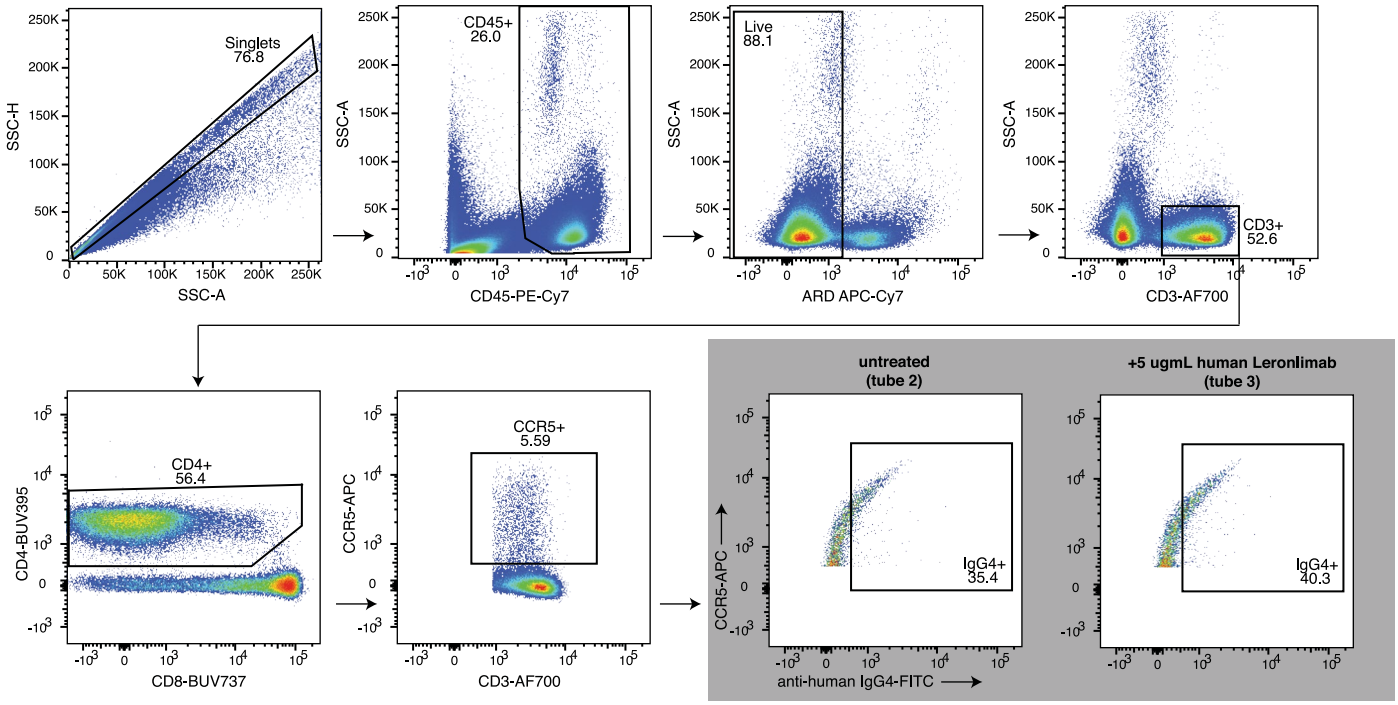

Extended Data Fig. 7 | Representative gating strategy for CD4 + T cell CCR5 receptor occupancy. For each tube, events were gated for CCR5 + CD4 + T cells by progressively gating on CD45 hi/mid, SSCA mid/lo, singlet, live, CD3+, CD4+, CCR5+ events. Figure shows example of a sample with 87.8% CCR5 RO. Details of CCR5 RO calculation are described in the Materials & Methods section.

https://doi.org/10.1038/s41564-026-02444-x

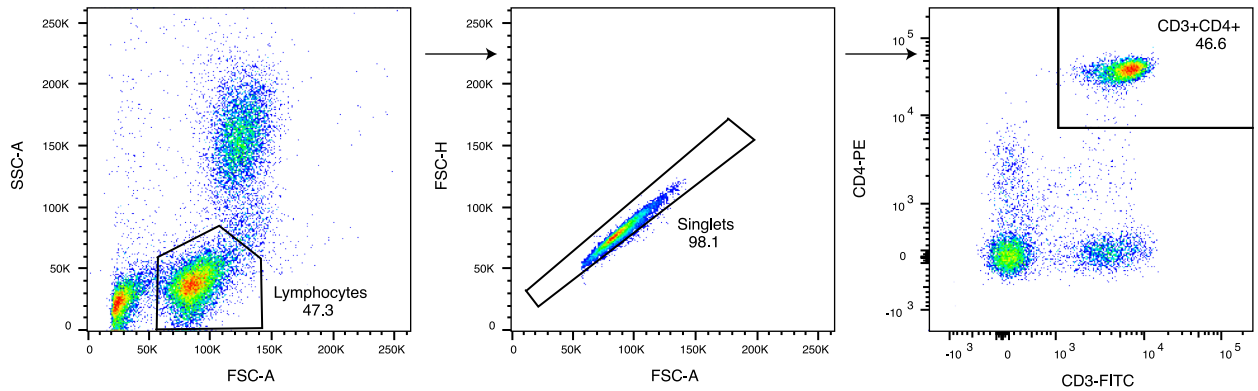

Extended Data Fig. 8 | Representative gating strategy for CD4 T cell counts. Events were gated for CD4 + T cells by progressively gating on lymphocytes (SSCA vs. FSCA), singlet, CD3 + CD4+ events.

nature portfolio

Corresponding author(s): Jonah B. Sacha and Nancy L. Haigwood

Last updated by author(s): Jun 16, 2026

Reporting Summary

Nature Portfolio wishes to improve the reproducibility of the work that we publish. This form provides structure for consistency and transparency in reporting. For further information on Nature Portfolio policies, see our Editorial Policies and the Editorial Policy Checklist.

Statistics

For all statistical analyses, confirm that the following items are present in the figure legend, table legend, main text, or Methods section.

n/a	Confirmed	
☐	☒	The exact sample size (*n*) for each experimental group/condition, given as a discrete number and unit of measurement
☐	☒	A statement on whether measurements were taken from distinct samples or whether the same sample was measured repeatedly
☐	☒	The statistical test(s) used AND whether they are one- or two-sided *Only common tests should be described solely by name; describe more complex techniques in the Methods section.*
☒	☐	A description of all covariates tested
☐	☒	A description of any assumptions or corrections, such as tests of normality and adjustment for multiple comparisons
☒	☐	A full description of the statistical parameters including central tendency (e.g. means) or other basic estimates (e.g. regression coefficient) AND variation (e.g. standard deviation) or associated estimates of uncertainty (e.g. confidence intervals)
☐	☒	For null hypothesis testing, the test statistic (e.g. *F*, *t*, *r*) with confidence intervals, effect sizes, degrees of freedom and *P* value noted *Give P values as exact values whenever suitable.*
☒	☐	For Bayesian analysis, information on the choice of priors and Markov chain Monte Carlo settings
☒	☐	For hierarchical and complex designs, identification of the appropriate level for tests and full reporting of outcomes
☒	☐	Estimates of effect sizes (e.g. Cohen's *d*, Pearson's *r*), indicating how they were calculated

Our web collection on statistics for biologists contains articles on many of the points above.

Software and code

Policy information about availability of computer code

Data collection	BD FACSDiva version 6.1 (BD Biosciences, San Jose, CA, USA) for flow cytometry. Gen5 v3.09 for ELISA plate reading. SoftMax Pro version 5.4 (Molecular Devices LLC, San Jose, CA, USA) for reading ELISA microplates
Data analysis	FlowJo (Tree Star, Inc), version 10.10.0; Excel v15.24 (Microsoft Inc., Redmond, WA, USA) GraphPad Prism (GraphPad Software), version 10.2.3

For manuscripts utilizing custom algorithms or software that are central to the research but not yet described in published literature, software must be made available to editors and reviewers. We strongly encourage code deposition in a community repository (e.g. GitHub). See the Nature Portfolio guidelines for submitting code & software for further information.

Data

Policy information about availability of data

All manuscripts must include a data availability statement. This statement should provide the following information, where applicable:

- Accession codes, unique identifiers, or web links for publicly available datasets
- A description of any restrictions on data availability
- For clinical datasets or third party data, please ensure that the statement adheres to our policy

All datasets generated and analysed during this study are included in this published article and its supplementary information files. Raw data files are available from the corresponding author on reasonable request.

Research involving human participants, their data, or biological material

Policy information about studies with human participants or human data. See also policy information about sex, gender (identity/presentation), and sexual orientation and race, ethnicity and racism.

Reporting on sex and gender	n/a
Reporting on race, ethnicity, or other socially relevant groupings	n/a
Population characteristics	n/a
Recruitment	n/a
Ethics oversight	n/a

Note that full information on the approval of the study protocol must also be provided in the manuscript.

Field-specific reporting

Please select the one below that is the best fit for your research. If you are not sure, read the appropriate sections before making your selection.

☒ Life sciences ☐ Behavioural & social sciences ☐ Ecological, evolutionary & environmental sciences

For a reference copy of the document with all sections, see nature.com/documents/nr-reporting-summary-flat.pdf

Life sciences study design

All studies must disclose on these points even when the disclosure is negative.

Sample size	Sample sizes were calculated assuming a 2-sided hypothesis test, with 80% power and alpha=0.05. The number of macaques needed in each experimental group to be able to detect significant differences in PVL have been determined. Experimental parameters were modeled using the virus stock SHIVSF162P3 in M. mulatta newborns, n=6. Week 2 data are used for the peak PVL in the controls (mean=7.650 log10 and SD=0.486 log10), and week 12 PVL for the set point (mean=6.456 log10 and SD=1.631 log10). Sample size needed in each group to see a halving of the set point viral load (i.e., a drop on average to 3.26 log10) is six.
Data exclusions	No data were excluded from the analyses.
Replication	Replicated data are noted in the description for each assay in Methods. Each assay was run with a validated standard. Contemporaneous controls were included in all experiments, and bNAb + ART experiments were replicated at different institutions at different times.
Randomization	Assignment to study groups was done as animals were born and the animals were not randomized.
Blinding	Animal care technicians, veterinarians, and investigators assessing and documenting pathology were blinded to the animals' group assignments. Analyses of viral quantification in blood and tissues (plasma viral copies by ddPCR; DNA in blood and tissues by ddPCR; and IPDA on enriched CD4 cells by magnetic selection) were performed on samples that were coded and blinded to the laboratory performing the assays.

Reporting for specific materials, systems and methods

We require information from authors about some types of materials, experimental systems and methods used in many studies. Here, indicate whether each material, system or method listed is relevant to your study. If you are not sure if a list item applies to your research, read the appropriate section before selecting a response.

Materials & experimental systems

n/a	Involved in the study
☐	☒ Antibodies
☒	☐ Eukaryotic cell lines
☒	☐ Palaeontology and archaeology
☐	☒ Animals and other organisms
☒	☐ Clinical data
☒	☐ Dual use research of concern
☒	☐ Plants

Methods

n/a	Involved in the study
☒	☐ ChIP-seq
☐	☒ Flow cytometry
☒	☐ MRI-based neuroimaging

Antibodies

Antibodies used	Purified human antibodies VRC07-523-LS and PGT121 were provided by the Vaccine Research Center, NIAID, NIH; anti-CD8alpha depleting antibody (mouse/rhesus CDR-grafted IgG1, clone M-T807R1) was sourced from NHP Reagent Resource, NIH; anti-CD3 (SP34-2: Alexa700, BD Biosciences, 624041, 100 ng per test; and Pacific Blue, BD Biosciences, 624034, 100 ng per test), anti-CD4 (L200: BV786, Fisher Scientific, BDB56531, 220 ng per test; BV510, BD Biosciences, 624340, 220 ng per test; BUV395, BD Biosciences, 624165, 220 ng per test; APC-Cy7, BD Biosciences, 564107), anti-CD8α (SK1: PerCP-eFluor710, Life Tech, CUST04424, 8 ng per test; BUV737, BD Biosciences, 612754,), anti-TNF-α (MAB11: FITC, BioLegend, 624046, 20 ng per test; and PE, BioLegend, 96019, 20 ng per test), anti-IFN-γ (B27: APC, BioLegend, 96018, 80 ng per test), anti-CD69 (FN50: PE, eBioscience, CUST01282, 50 ng per test; and PE/Dazzle594, BioLegend, 93437, 50 ng per test), anti-CD45 (D058-1283: PE Cy7, BD Biosciences, 561294, 200 ng per test), anti-CCR5 (J418F1: APC, 359122, Biolegend, 100 ng per test), live/dead near IR (L-34976, Invitrogen), live/dead yellow (L-34959, Invitrogen), human IgG4 (HP-6025: FITC, F9890, Sigma, 3:100)
Validation	These antibodies are well validated and the details can be found at the nonhuman primate reagent resource website. Antibodies used for flow cytometry were validated by the manufacturer and titrated on rhesus macaque cells and human cells in-house at Vaccine & Gene Therapy Institute at OHSU (Hansen et al., Nature 2013).

Animals and other research organisms

Policy information about studies involving animals; ARRIVE guidelines recommended for reporting animal research, and Sex and Gender in Research

Laboratory animals	Rhesus macaques (Macaca mulatta) were included in this study. These are outbred populations. Both male and female infants were included.
Wild animals	This study did not involve wild animals.
Reporting on sex	Sex was not considered as part of the study design because we have extensive data published showing that both male and female infant macaques are equivalently affected by SHIV-SF162P3 oral infection when infected as infants (4 weeks of age or less). Animals were assigned to groups 3-4 weeks after they were born, and it was not always possible to balance exact numbers of males and females. Sex as a variable is not required for nonhuman primate studies.
Field-collected samples	The study did not involve field-collected samples.
Ethics oversight	This study used outbred Indian origin rhesus macaques (Macaca mulatta) from the type D retrovirus-, simian immunodeficiency virus-, and simian lymphocyte tropic virus type 1-free breeding colonies of the Oregon National Primate Research Center (ONPRC) and the California National Primate Research Center (CNPRC). All experimental procedures were IACUC approved and conducted at ONPRC or CNPRC, both of which are accredited by the Association for Assessment and Accreditation of Laboratory Animal Care International (AAALAC). Animal care followed the guidelines outlined in the 2011 Guide for the Care and Use of Laboratory Animals by the Institute for Laboratory Animal Research. Full details of IACUC study protocols, approved at each institution, are included in the manuscript. IACUC approval number is 23302.

Note that full information on the approval of the study protocol must also be provided in the manuscript.

Plants

Seed stocks	n/a
Novel plant genotypes	n/a
Authentication	n/a

Flow Cytometry

Plots

Confirm that:

☒ The axis labels state the marker and fluorochrome used (e.g. CD4-FITC).

☒ The axis scales are clearly visible. Include numbers along axes only for bottom left plot of group (a 'group' is an analysis of identical markers).

☒ All plots are contour plots with outliers or pseudocolor plots.

☒ A numerical value for number of cells or percentage (with statistics) is provided.

Methodology

Sample preparation	The sample preparation is described in sufficient detail to fully recapitulate the process in the methods under the following sections: blood and biopsy samples, in vivo CD8+ cell depletion, intracellular cytokine staining, measurements of Leronlimab in plasma, CCR5 RO on cells, and ant0-drug antibodies.
Instrument	BD LSR II Flow Cytometer, BD FACSymphony A5 Flow Cytometer
Software	Collected using BD FACSDiva v8.01 and analyzed using Flow Jo (Tree Star, Inc.), version 10.10.0
Cell population abundance	No cell sorting was performed.
Gating strategy	Gating strategies for CCR5 receptor occupancy have been previously described and published in the following: Chang XL, Wu HL, Webb GM, Tiwary M, Hughes C, Reed JS, Hwang J, Waytashek C, Boyle C, Pessoa C, Sylwester AW, Morrow D, Belica K, Fischer M, Kelly S, Pourhassan N, Bochart RM, Smedley J, Recknor CP, Hansen SG, Sacha JB. CCR5 Receptor Occupancy Analysis Reveals Increased Peripheral Blood CCR5+CD4+ T Cells Following Treatment With the Anti-CCR5 Antibody Leronlimab. Front Immunol. 2021 Nov 19;12:794638. doi: 10.3389/fimmu.2021.794638. PMID: 34868084; PMCID: PMC8640501. Gating strategies are also provided in Extended Figures 6, 7, 8.

☒ Tick this box to confirm that a figure exemplifying the gating strategy is provided in the Supplementary Information.